INORGANIC / POLYMERIC ASSEMBLIES AS CATALYSTS FOR WATER SPLITTING

A THESIS SUBMITTED TO
THE GRADUATE SCHOOL OF ENGINEERING AND SCIENCE
OF BILKENT UNIVERSITY
IN PARTIAL FULFILLMENT OF THE REQUIREMENTS FOR
THE DEGREE OF
MASTER OF SCIENCE
IN
CHEMISTRY

By
Zeynep Kap
September 2018

Inorganic / Polymeric Assemblies as Catalysts for Water Splitting
By Zeynep Kap
September 2018

We certify that we have read this thesis and that in our opinion it is fully adequate, in scope and in quality, as a thesis for the degree of Master of Science.

Ferdi Karadaş(Advisor)

Emrah Özensoy

Yavuz Dede

Approved for the Graduate School of Engineering and Science:

Ezhan Karaşan
Director of the Graduate School

ABSTRACT

INORGANIC / POLYMERIC ASSEMBLIES AS CATALYSTS FOR WATER SPLITTING

Zeynep Kap
M.S. in Chemistry
Advisor: Ferdi Karadaş
September 2018

Splitting water with sunlight is an attractive and promising research topic over the last two decades since it produces a non-carbon-based resource, hydrogen, which is a suitable energy carrier due to its high energy output and for being environmentally friendly. A great deal of research in this field has been centered on the development of efficient water oxidation and reduction catalysts.

The first part of the thesis focuses on a novel photosensitizer-water oxidation catalyst (PS-WOC) dyad. A Ru metal coordinated pyridine-based ligand and a cobalt-iron pentacyanoferrate have been used as the photosensitizer and water oxidation catalyst, respectively. In this assembly, poly(4-vinylpyridine) serves as the bridging group between two units mainly to enhance the performance and stability of the system compared to its analogous intermolecular system. A 5-fold improvement on the catalytic activity has been achieved with a turnover frequency (TOF) of 5.6×10^{-4} s^{-1} under 1 hour light illumination and a turnover number (TON) of 11 in a 6-hour catalytic study. Evolved oxygen was quantified with gas chromatography. Structural characterization was carried out by Fourier Transform Infrared Spectroscopy (FTIR), Ultraviolet-Visible Spectroscopy (UV-Vis), X-Ray Photoelectron Spectroscopy (XPS), X-Ray Powder Diffraction (XRD), Scanning Electron Microscopy (SEM), and Energy-dispersive X-Ray Spectroscopy (EDX) techniques. Comparative XPS and FTIR studies were performed on pristine and post-catalytic samples to confirm the stability of the dyad.

In the second part of the study, a facile synthetic pathway using poly(4-vinylpyridine) as a polypyridyl platform has been reported for the formation of

a cobalt-based metallopolymer. Electrochemical studies indicate that the metallopolymer acts as an efficient H_2 evolution catalyst similar to cobalt-polypyridyl complexes. Furthermore, metallopolymer can be transformed to cobalt particles when a cathodic potential is applied in the presence of an acid. It has been found that these cobalt particles also serve as efficient hydrogen evolution catalysts. Approximately 80 μmoles of H_2 gas can be collected during 2 h of electrolysis at -1.5 V (vs. $Fc^{+/0}$) in the presence of 60 mM of acetic acid. A comprehensive study of the electrochemical and electrocatalytic behavior of cobalt–poly(4-vinylpyridine) was discussed in detail.

Keywords: Water reduction catalyst, Hydrogen evolution catalyst, Light-driven water oxidation catalyst, Light-driven oxygen evolution catalyst, Dyad, Water splitting, Ruthenium, Prussian Blue, Polymer.

ÖZET

SUYUN AYRIŞMA REAKSİYONU İÇİN İNORGANİK / POLİMERİK YAPILI KATALİZÖRLER

Zeynep Kap
Kimya, Yüksek Lisans
Tez Danışmanı: Ferdi Karadaş
Eylül 2018

Güneş ışığı ile suyun ayrışması, yenilenebilir enerji arayışı sürecinde son yıllarda sıklıkla çalışılan ve gelecek vadeden bir araştırma konusudur çünkü reaksiyon sonucunda üretilen hidrojen, yüksek enerji üretimi ve çevre dostu olması nedenleriyle uygun bir enerji taşıyıcısıdır. Bu nedenle bu alanda hatırı sayılır sayıda araştırma suyu yükseltgeyen ve indirgeyen verimli katalizör yapıları bulmaya odaklanmıştır.

Bu tezin birinci bölümünde, özgün bir kromofor-suyu yükseltgeyen katalizör (PS-WOC) dyad sistemi geliştirilmiştir. Kromofor birimi olarak rutenyum metal koordinasyonlu piridin merkezli ligand kullanılırken, suyu yükseltgeyen katalizör olarak ise kobalt-demir bazlı Prusya mavisi analoğu kullanılmıştır. Bu yapıda, poli(4-vinilpiridin) iki farklı görevi olan birimleri birbirine bağlayan bir moleküler köprü görevi görmektedir ve inter-moleküler örneği ile kıyaslandığında, aktiviteyi ve kararlılığı arttırdığı gösterilmiştir. Katalitik aktivitenin 5 kat arttığı gözlemlenmiştir ve 1 saat ışık altında, TOF 5.6×10^{-4} sn^{-1}, 6 saatlik dilimde ise TON 11 bulunmuştur. Oluşan oksijen, gaz kromatografisi ile ölçülmüştür. Yapısal karakterizasyon, Fourier Dönüşümlü Kızılötesi (FTIR) Spektrometresi, UV-Vis Spektrometresi (UV-Vis), X-Ray Spektrometresi (XPS), X-Ray Difraksiyonu (XRD), Taramalı Elektron Mikroskobu (SEM) ve Enerji Dağılımlı X-Işını Spektroskopisi (EDX) teknikleri ile yapılmıştır. Karşılaştırmalı XPS ve FTIR çalışmaları yapılarak ise, katalitik aktivite öncesi ve sonrasına bakılmış, yapının kararlılığı kanıtlanmıştır.

Çalışmanın ikinci bölümünde, poli(4-vinilpiridin)'in polimer platformu olarak kullanıldığı, basit bir şekilde sentezlenen kobalt bazlı metal-polimer rapor

edilmiştir. Elektrokimyasal ölçümler sonucu, sentezlenen metal-polimerin literatürdeki kobalt-polipiridil örnekleri gibi suyun indirgenmesi (H_2 oluşumu) katalizörü olarak verimli olduğu görülmüştür. Bunun yanı sıra, metal-polimerin asidik ortamda ve katodik potansiyel uygulandığında kobalt parçacıklarına dönüştüğü saptanmıştır ve bu kobalt parçacıklarının da H_2 oluşumu katalizörü olarak verimli olduğu gözlenmiştir. Çalışma sonucu, 2 saatlik elektroliz sürecinde, -1.5 V potansiyelde (vs. $Fc^{+/0}$) ve 60 mM asetik asit ortamında yaklaşık 80 μmol H_2 toplanmıştır. Kapsamlı bir çalışma ile kobalt-poli(4-vinilpiridin)'in elektrokimyasal ve elektrokatalitik karakterizasyonu ele alınmıştır.

Anahtar sözcükler: Suyun katalitik indirgenmesi, Hidrojen oluşumu katalizörü, Işık kaynaklı suyun katalitik yükseltgenmesi, Işık kaynaklı oksijen oluşumu katalizörü, Dyad, Suyun ayrıştırılması, Rutenyum, Prusya Mavisi, Polimer.

Acknowledgement

I owe my sincere gratitude to Asst. Prof. Ferdi Karadaş because his encouragement has been the asset for starting my research journey. At that time, I could not imagine how this decision can shape me in so many ways that I cannot begin to list. I am grateful to him for giving me the opportunity to work under his supervision and for his progressive guidance and advice throughout my study. One simply could not wish for a friendlier supervisor that is also a brilliant scientist.

I appreciate the feedback offered by the thesis committee members, Emrah Özensoy and Yavuz Dede. Also, I would like to thank staff members of Chemistry Department which I gratefully benefited from their knowledge and experience. Especially, I received generous support from Asst. Prof. Bilge Baytekin and thanks to the fruitful comments and discussions she offered, I accomplished my project.

I am thankful to TÜBİTAK for their financial support during my research. (Project no: 215Z249)

I could not end this section without conveying my gratitude to current and former Karadas group members, Emine Ülker, Satya Vijaya Kumar Nune, Gamze Türkan Ulusoy Ghobadi, Sina Sadigh Akbari and Pınar Alsaç for their accompany during the course of my study, their friendship and help. Especially, without the contribution and support of Emine Ülker and Satya Vijaya Kumar Nune my research would not have been possible. Special thanks to Sina Sadigh Akbari for his kindness and support, especially during photocatalytic measurements. I would also like to thank Ethem Anber whose services are highly appreciated.

Finally yet importantly, I must express my deepest gratitude to my family for providing continuous support and trust throughout my entire life. I must also acknowledge the support and help offered by my friends, especially by Doğancan Dinler, which kept me motivated even in the tough moments.

Contents

List of Figures

List of Tables

Abbreviations

ν	Scan rate
μ	Micro
A	Ampere
V	Volts
eV	Electron volts
I_c	Catalytic current
I_p	Peak current
I	Current
j	Current density
j_0	Exchange current density
λ	Wavelength
Å	Angstrom
h	Hour
$Fc^{+/0}$	Ferrocenium/ferrocene couple
(v/v)	% volume per volume
ϵ	Molar absorptivity
AcOH	Acetic acid
$CoAc_2$	Cobalt acetate
CV	Cyclic voltammogram
EDX	Energy-Dispersive X-Ray Spectroscopy (EDX)
FTIR	Fourier Transform Infrared Spectroscopy
FWHM	Full width at half maximum
FTO	Fluorine-doped tin oxide

GC	Gas chromatography
GCE	Glassy carbon electrode
LSV	Linear sweep voltammetry
MeCN	Acetonitrile
P4VP	Poly(4-vinylpyridine)
PBA	Prussian Blue Analogue
PS	Photosensitizer
SEM	Scanning Electron Microscopy
TOF	Turnover frequency
TON	Turnover number
UV-Vis	UV-Visible Spectroscopy
WOC	Water oxidation catalyst
XPS	X-Ray Spectroscopy
XRD	X-Ray Diffraction

Chapter 1

Introduction

In this chapter, part 1.4 is based on the publication "Electrocatalytic hydrogen evolution with cobalt–poly(4-vinylpyridine) metallopolymers", Zeynep Kap; Emine Ülker; Satya Vijaya Kumar Nune; Ferdi Karadas, Journal of Applied Electrochemistry, 2018, 48 (2): 201-209. "Reprinted by permission from Springer Nature. Copyright 2018, Journal of Applied Electrochemistry.

1.1 Solar Energy as an Alternative for Fossil Fuel

With recent technological developments and increasing world population, global energy demand cannot be met using fossil fuels such as petroleum, coal, and natural gas.[1] From past to present, fossil fuels have been the primary energy source although they are limited and side products such as oxides of carbon, nitrogen, sulfur, and etc. are produced, which are the main cause of global warming we are facing today.[2] Hydrogen appears to be the most prominent solution that can be used in industrial systems as an energy carrier since it possesses inherent high specific energy, and moreover it doesn't lead any pollutant emissions.[1],[3]

Hydrogen can be produced from various renewable resources including hydro, wind, biomass, geothermal, and solar.[4] Of these, solar energy is the most promising and sustainable one, according to US Department of Energy report in 2004. Solar energy is mainly based on splitting water using light as an energy input. Hence, many research efforts have addressed to develop a system that is capable of converting solar energy into chemical energy efficiently.

1.2 Artificial Photosynthesis

Photosynthesis is the process of photochemical conversion and storage of solar energy in photosynthetic organisms, whereas artificial photosynthesis is based on mimicking the photosynthetic reactions.[5] It is crucial to understand the mechanism behind natural photosynthesis to design such systems.

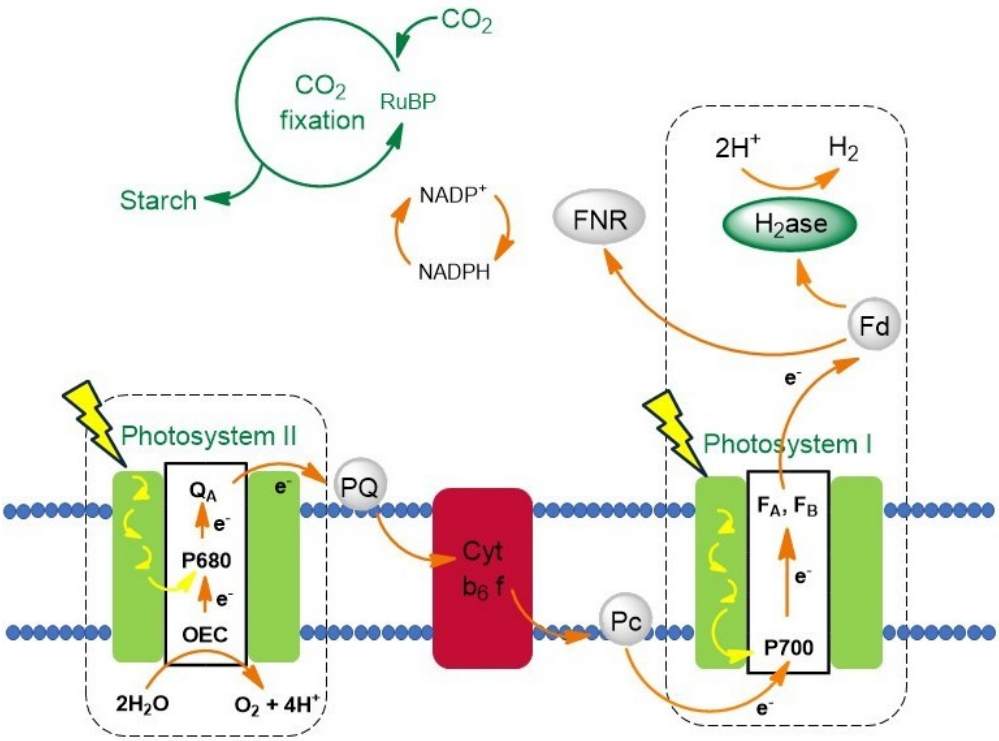

Figure 1.1: Schematic representation of the photosynthetic chain in the oxygenic photosynthesis.[6]

The process is initiated in photosystem II (PS II) where O_2 is catalytically produced upon photooxidation of H_2O. This process is followed by the migration of electrons to photosystem I (PS I), where a second light harvesting process occurs to produce H_2 eventually.[6] In plants, H_2 is combined with CO_2 to produce sugar, on the other hand, some organisms such as cyanobacteria and microalgae have a unique enzyme called hydrogenase, which releases H_2 (Figure 1.1).[7]

During the photosynthetic process, oxygen production is catalyzed by an oxygen-evolving $CaMnO_4$ center (OEC) in PS II and hydrogen production is catalyzed by dinuclear metal clusters available in hydrogenase.[6] As shown in Figure 1.2, the OEC unit consists of three manganese, one calcium, and four oxygen atoms forming a cubane-like structure. The fourth manganese site is linked to two manganese atoms by oxo-biridges.[8] This cluster collects four hole equivalents by light excitation of PS II, and thus accomplishes water oxidation.[9] Inspired by this structure, water oxidation catalysts (WOCs) are mainly based on Ru, Mn, Ir, and Co metals with hard ligands such as O- and N-rich ligands.[8],[10]

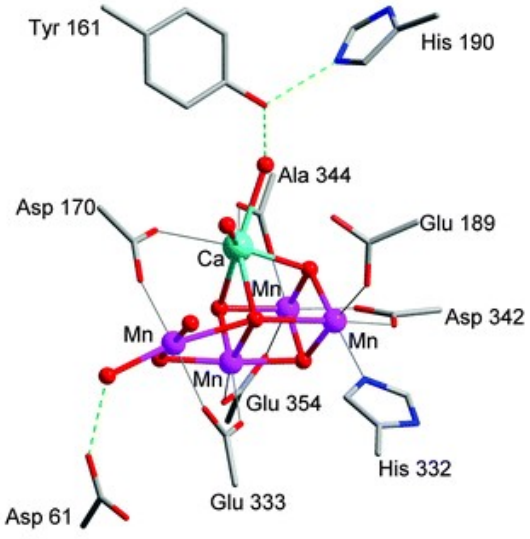

Figure 1.2: Structure of the Mn_4CaO_5 cluster and its ligand environment.[8] Adapted by permission of The Royal Society of Chemistry.

On the other hand, hydrogenase enzymes have active sites either based on

nickel and iron metals or iron only where both atoms are surrounded with sulfur containing ligands and coordinated to cyanide and carbon monoxide groups (Figure 1.3). Catalysts containing Fe, Co, and Ni ions have been widely studied with strong electron accepting ligands such as sulfides and phosphines.[11] Despite all the achievements obtained with 3d-transition metal ions, platinum appears to be the best catalyst known to date.

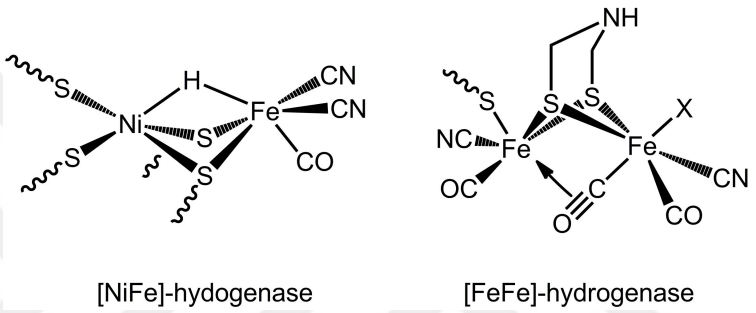

Figure 1.3: Structure of the active sites of [NiFe]-hydrogenase in the Ni-C state and of [FeFe]-hydrogenase in the reduced active state (X is a either a water molecule or a H_2 ligand).[6]

Majority of the current research is centered on adopting basic design principles in natural photosynthesis. Photosynthesis is a highly efficient system since it involves two light harvesting units and charge recombination is prevented by the unique electron transfer chain. Therefore, the insights of the complex multi-electron redox transfer is an inspiration to develop analogue models.

The main objective with water splitting is to convert solar light into chemical energy and concurrently to produce hydrogen and oxygen. The process consists of two half reactions; water oxidation and water reduction (Figure 1.4).

$$O_2 + 4H^+ + 4e^- \rightleftharpoons 2H_2O \qquad E_{anodic} = 1.23\ V - 0.059\ V \times (pH)\ vs.\ NHE$$

$$4H^+ + 4e^- \rightleftharpoons 2H_2 \qquad E_{cathodic} = 0\ V - 0.059\ V \times (pH)\ vs.\ NHE$$

$$2H_2O \longrightarrow 2H_2 + O_2 \qquad E_{reaction} = -1.23\ V$$

Figure 1.4: Half-cell reactions and the reduction potentials of electrolysis of water.

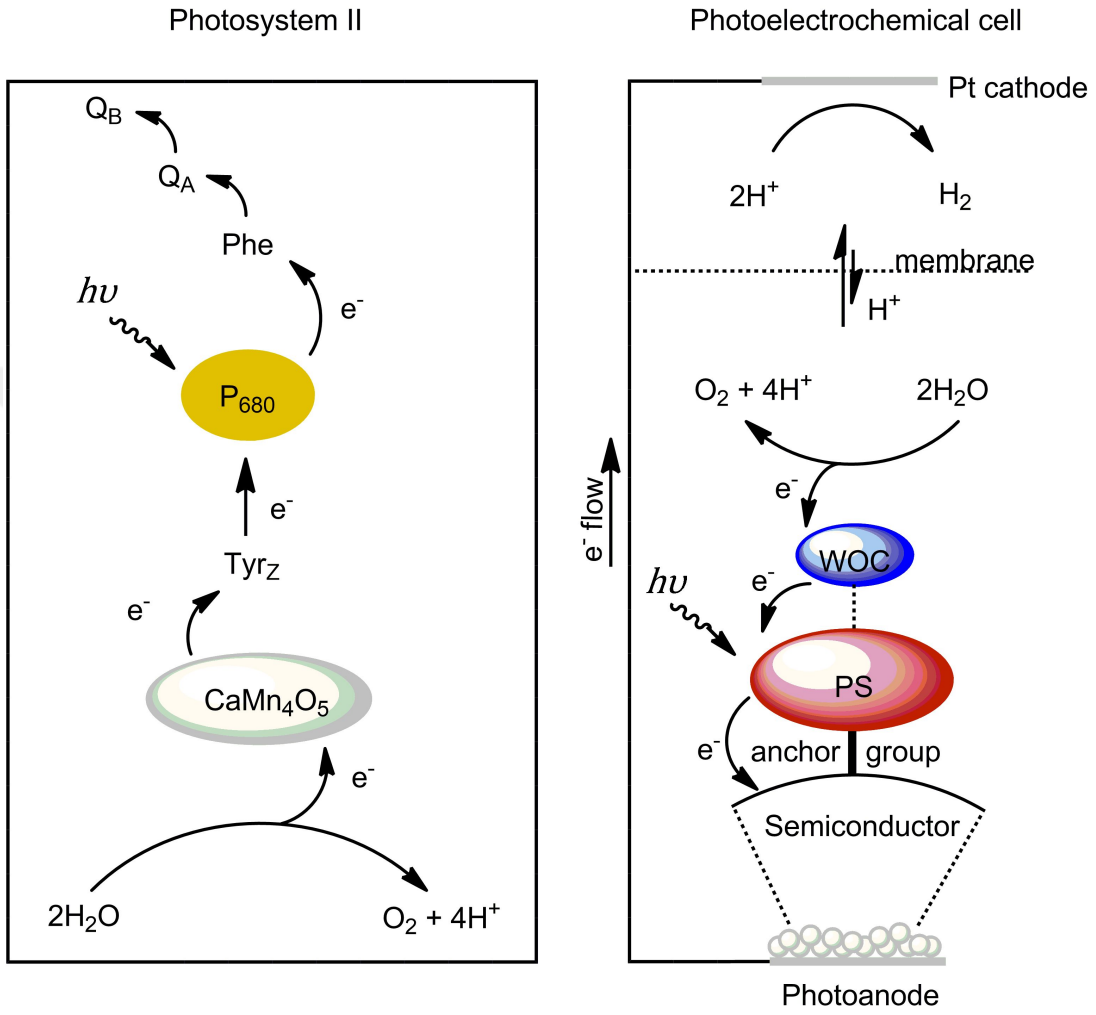

Figure 1.5: Schematic representation of (i) electron transfer sequence in PS II and (ii) working principle of a photoelectrochemical cell.[8] Photosensitizer is abbreviated as PS and water oxidation catalyst is abbreviated as WOC. Reproduced by permission of The Royal Society of Chemistry.

Photoelectrochemical cells (PEC) are designed to achieve solar-driven water splitting and their working principle is derived from natural photosynthesis.[9] As in nature, required potential to stimulate the reaction is supplied by sunlight. Photosensitizer (PS) absorbs light, which is anchored to either anode or cathode and through electron transfer, hydrogen and oxygen are generated in different media separated by a membrane (Figure 1.5). Two half reactions are connected through an external electron flow.

The “antennae” alignment of pigments is observed in natural photosynthesis which is responsible from the collection of energy of photons and transfer of generated holes/electrons to the final donor/acceptor.[6] Charge separation is achieved in a way to facilitate energy storing reactions and to minimize backward reactions.[6][7] Although the challenge still remains, it is crucial to design systems that are capable of transporting holes/electrons to the final donor/acceptor without back-electron transfer, which would lead a charge recombination (Figure 1.6).

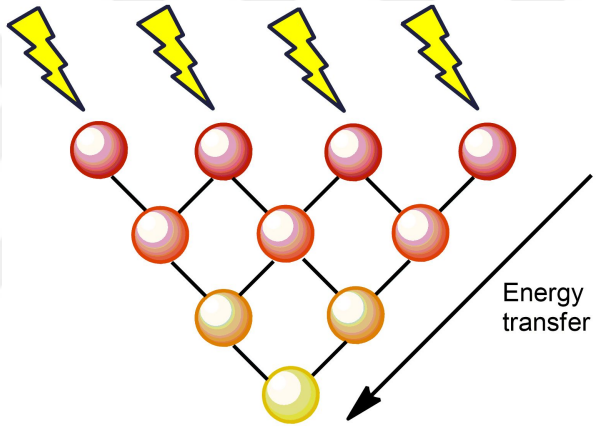

Figure 1.6: Schematic illustration for light-harvesting array mimicking in artificial photosynthesis; the collection and transport of energy.[6]

Supramolecular systems are designed to serve as molecular light harvesting arrays that involve electron acceptors (A) and donors (D) to mimic the energy transfer cascade in natural photosynthesis.[6] These systems are developed by the combination of a photosensitizer and a suitable catalyst for water reduction and water oxidation with electron donor/acceptor pairs (Figure 1.7).[6]

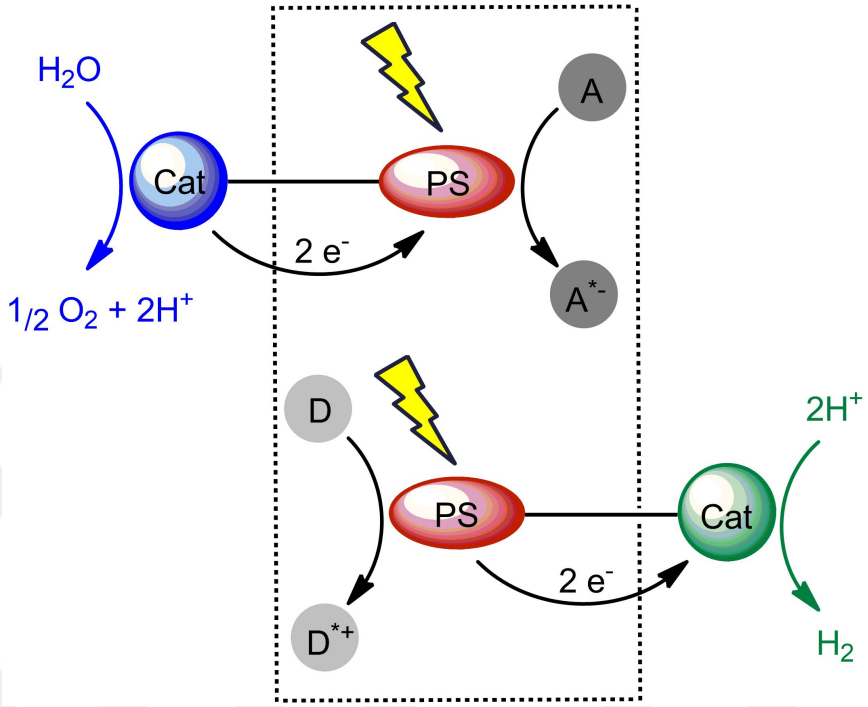

Figure 1.7: Schematic representation of homogeneous multielectron photocatalysis for light-driven water splitting.[6] Abbreviations used are as follows: PS is photosensitizer, Cat is catalyst, D is donor and A is acceptor.

1.3 Water Oxidation with Photosensitizer-Catalyst (Dyad) Assemblies

While separate molecular systems serve as a PS and WOC in earlier studies, recently dyads, in which the molecular PS and WOC are connected to each other with a suitable linker, have been developed to enhance the electron transfer between molecular units.[12],[13],[14],[15] In PEC systems, these supramolecular systems have a practical advantage on overcoming charge transport kinetics between the units. Ru(II) based PS-WOC assemblies showed %22 and %74 faradaic efficiency for O_2 production on TiO_2 in dye-sensitized photoelectrochemical cell (DSPEC) systems, respectively (Figure 1.8).[16],[17]

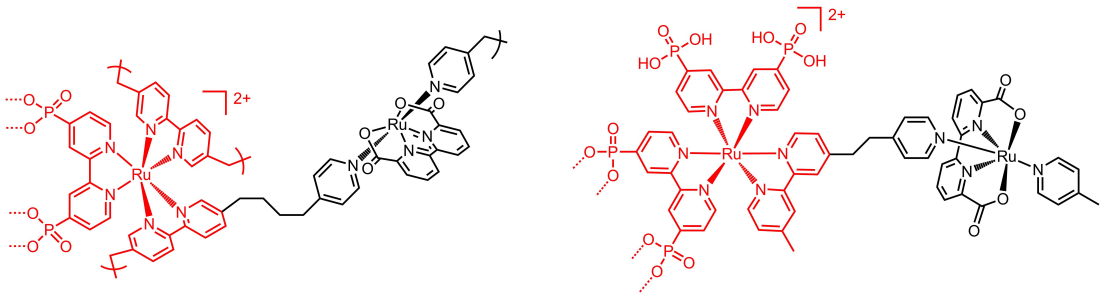

Figure 1.8: Examples of PS-WOC assemblies designed for DSPEC systems.[16],[17] PS unit of the assemblies are demonstrated as red in the structures.

There are several studies that the catalytic efficiency of the dyad systems was investigated in homogeneous solution. Thummel et al. reported that Ru-Ru dyad assembly showed a TON of 134 under 6 h light illumination, which is far more higher than its analogous intermolecular system with a TON of 6.[13] A follow-up study by Thummel et al. showed how the efficiency is affected by performing component analysis on several dyads (Figure 1.9). The most active assembly showed a TON of 68 under 1 h light illumination in the presence of sodium persulfate at pH 5.3.[18] Licheng Sun et al. also focused on PS-WOC assemblies, incorporating a ruthenium diimine chromophore and ruthenium based catalyst.[19] TON of the assembly was found as 38 where the separate system showed TON of 8 which indicates a significant enhancement of catalytic activity.

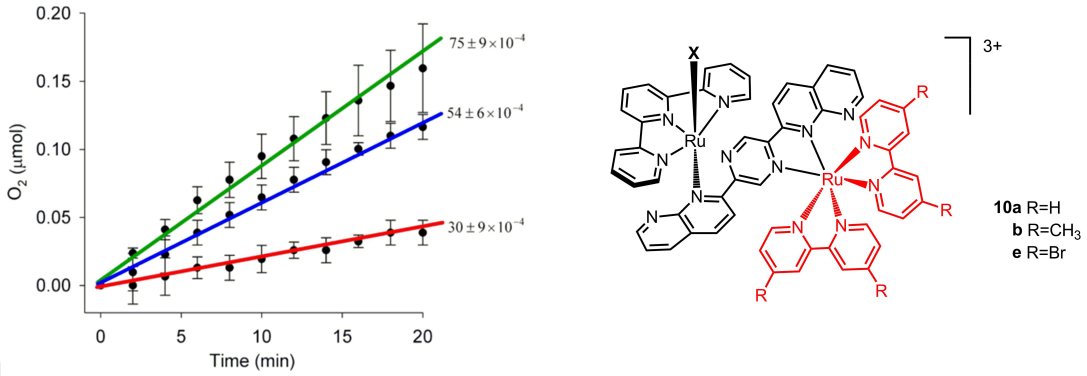

Figure 1.9: Graph of O_2 vs. Time for dyads 10a (blue), 10b (red), and 10e (green) with their related initial rates (μmol/min with error bars) given. PS unit of the assembly is demonstrated as red in the structure. "Reprinted with permission from [19]. Copyright 2014, American Chemical Society".

In majority of the dyad systems, ruthenium based units have been preferred as both PS and WOC due to their strong light absorption, long excited state lifetimes, and high efficiencies.[20] However, entirely earth-abundant dyads should be investigated to replace ruthenium since it is one of the rarest metals on earth. In this regard, Licheng Sun et al. investigated a dyad which utilizes a Co_4O_4 cubane system as a WOC (Figure 1.10). The study shows that the Ru–Co dyad has a TON of 5, and it is significantly more active than that of a multicomponent system.[21] The higher activity of the assembly is attributed to the stability of the assembly and particularly the stabilization of the chromophore, which is achieved by intramolecular electron transfer.

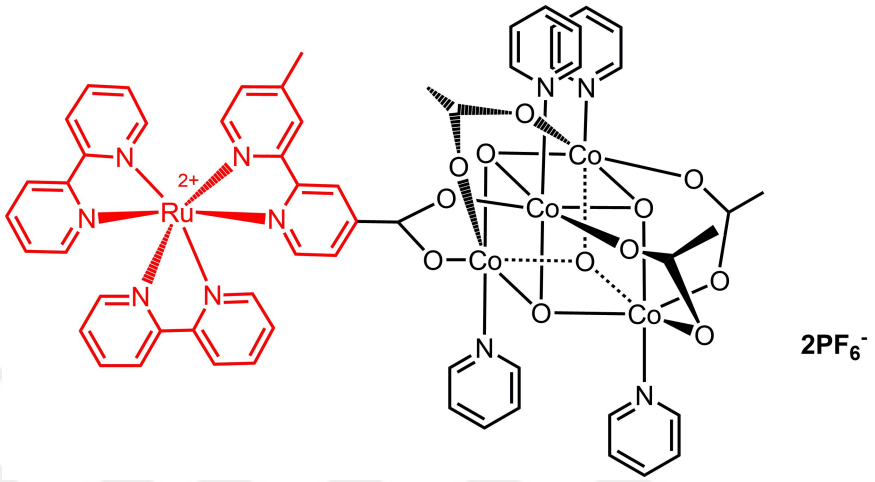

Figure 1.10: Structure of ruthenium chromophore-cobalt cubane assembly.[21] PS unit of the assembly is demonstrated as red in the structure.

Polymeric platforms have also been used to prepare dyads.[20],[22],[23],[24],[25] Several studies indicate that enhanced catalytic efficiency observed on polymeric dyad systems is due to a hopping mechanism along the chain, which results in an intra-assembly electron/hole transfer.[14],[24],[25] Waters et al. reported that an electrode-bound helical peptide PS-WOC assembly has 10-fold enhanced catalytic efficiency compared to its analogous homogeneous system (Figure 1.11).[23] It has been shown that intra-assembly electron transfer is a key process to enhance efficiency and alignment of the distance between units and that electron transfer rates can be optimized.[23],[24] Hisaeda et al., in their work, emphasized that an assembly with a polymer linkage can also efficiently work even under diluted conditions by fixation of each functional group in the same polymeric unit, thus, providing close distance for electron transfer.[26] Furthermore, in the presence of a polymeric support, stability of the system is expected to increase by preventing photodecompositon of the photosensitizer.[26],[27] Despite the aforementioned advantages, implementing earth-abundant components, particularly for the catalytic site, still remains a significant challenge.

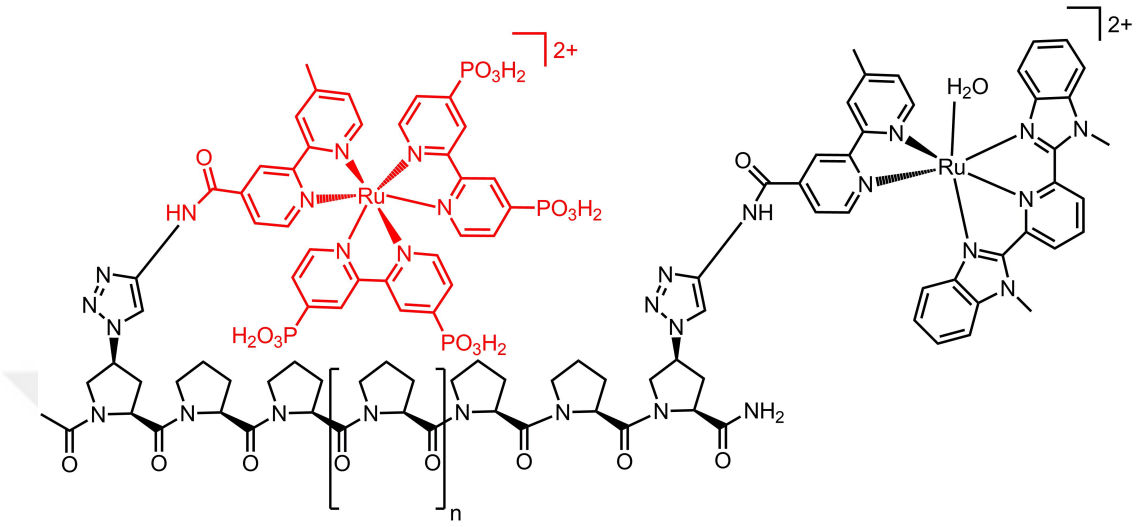

Figure 1.11: Structure of the PS-WOC metallopeptide.[23] PS unit of the assembly is demonstrated as red in the structure.

1.4 Water Reduction Electrocatalysts

A great deal of research has focused on the development of catalysts for hydrogen evolving reactions to use hydrogen as a clean energy carrier.[28],[29],[30],[31],[32][33],[34] Even though platinum is the best catalyst known to date, its high cost renders researchers to find alternative catalysts that are efficient and of great abundance. Catalysts containing Co and Ni have been the pioneers in this field since several electrocatalysts such as cobalt diglyoxime complexes also known as cobaloximes [35],[36],[37], cobalt diamine-dioximes [38], cobalt polypyridyl complexes [29],[34],[39],[40],[41] (Figure 1.12), nickel phosphines [28][42],[43],[44], and cobalt sulfides [45] are reported to evolve hydrogen from water efficiently.

Although molecular complexes have been the center of focus they tend to disintegrate under drastic electrocatalytic and photocatalytic conditions. For example, the debate on whether cobalt diamine-dioxime complexes degrade to form cobalt-containing nanoparticles is still ongoing. Kaeffer et al. recently

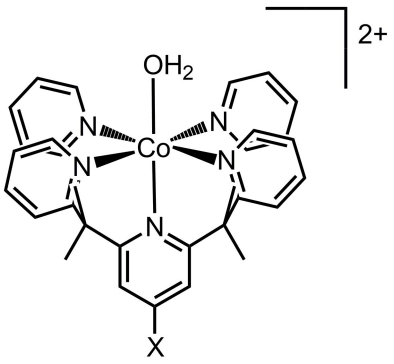

4 X = H
5 X = CF_3
6 X = NMe_2

Figure 1.12: Example of a cobalt-polypyridyl system as hydrogen evolution catalyst.[29]

claimed that molecular complexes act as molecular catalysts in non-aqueous solutions, while in acidic and/or aqueous solutions could transform to metal-based nanoparticles.[46] Recent studies that take advantage of such decomposition processes indicate that the nanoparticles that are produced from molecular complexes during electrocatalysis could also serve as efficient water reduction catalysts. The synthetic strategy including the use of molecular systems as precursors for electroactive nanoparticles for water reduction was first reported by Anxolabéhère-Mallart et al. in 2012.[47] The origin of the catalytic activity of an intensely studied cobalt clathrochelate system, in which cobalt site is buried inside a hexadentate ligand cavity, was one of the recent disputes among molecular hydrogen evolution catalysts since no catalytic activity was expected from such a sterically hindered cobalt site. It was found that, in fact, cobalt nanoparticles formed because of the decomposition of the molecular cobalt complex were responsible for electrocatalytic water reduction. A follow-up study on a series of cobalt-trisglyoximato complexes with different ligand sets showed that potential for electrodeposition is highly dependent on the type of the ligand.[48] A recent study by Anxolabéhère-Mallart et al. led to the conclusion that cobalt-bisglyoximato complex, which is not an active electrocatalyst for proton reduction, can be altered in the presence of acid to electroactive cobalt based nanoparticles for proton reduction.[49] Such an electrodeposition process was also observed not only

for cobalt complexes with different ligands such as pyridine oxime but also for metal complexes other than cobalt such as $[Ni(N–N–SCH_3)_2](BF_4)_2$(N–N–SCH = $2-$pyridyl$-$N$-(2'-$methylthiophenyl)methyleneimine).[50],[51]

The said deposits have two key advantages over molecular systems:

i) They don't require a further step to connect them on electrode since they are readily deposited on the electrode and

ii) They are much more stable compared to molecular systems under drastic electrocatalytic processes.

Therefore, the method involving the use of monometallic complexes as precursors to form water reduction catalysts should be investigated further.

1.5 Scope of the Study

In this thesis, catalysts for both water oxidation and water reduction have been designed, prepared, characterized and their catalytic performances have been investigated. These studies have been examined in two parts.

In the first part, a novel heterogeneous PS-WOC dyad, which incorporates poly(4-vinylpyridine) as a bridge between a ruthenium chromophore and cobalt-based PBA, has been presented. Cobalt-hexacyanometalates have recently been demonstrated as promising water oxidation catalysts due to their high catalytic activities, robustness, and stabilities at neutral pH.[52],[53] Therefore, the use Co-Fe PBAs as WOCs rather than Ru based WOCs will be a step forward in the development of entirely earth-abundant dyads. P4VP has recently been used to prepare Co-Fe coordination polymer as a water oxidation catalyst by our group.[54] The study indicates that $Fe(CN)_5$ groups can easily be coordinated to pyridyl groups of P4VP, which is a robust precursor for the formation of amorphous PBAs. In another study, Co-P4VP assembly has successfully been prepared and found to be an efficient in water reduction electrocatalyst.[55] The

studies showed that P4VP can be a convenient platform for catalytic applications. Herein, it is proposed a synthetically facile dyad, wherein the ruthenium-based molecular photosensitizer is connected to Prussian blue type WOC through a P4VP platform (Figure 1.13). It is the first study that the photocatalytic activity of a polymeric dyad system is investigated in a homogeneous solution. Stability and efficiency of the assembly is presented with various characterization techniques and photocatalytic measurements.

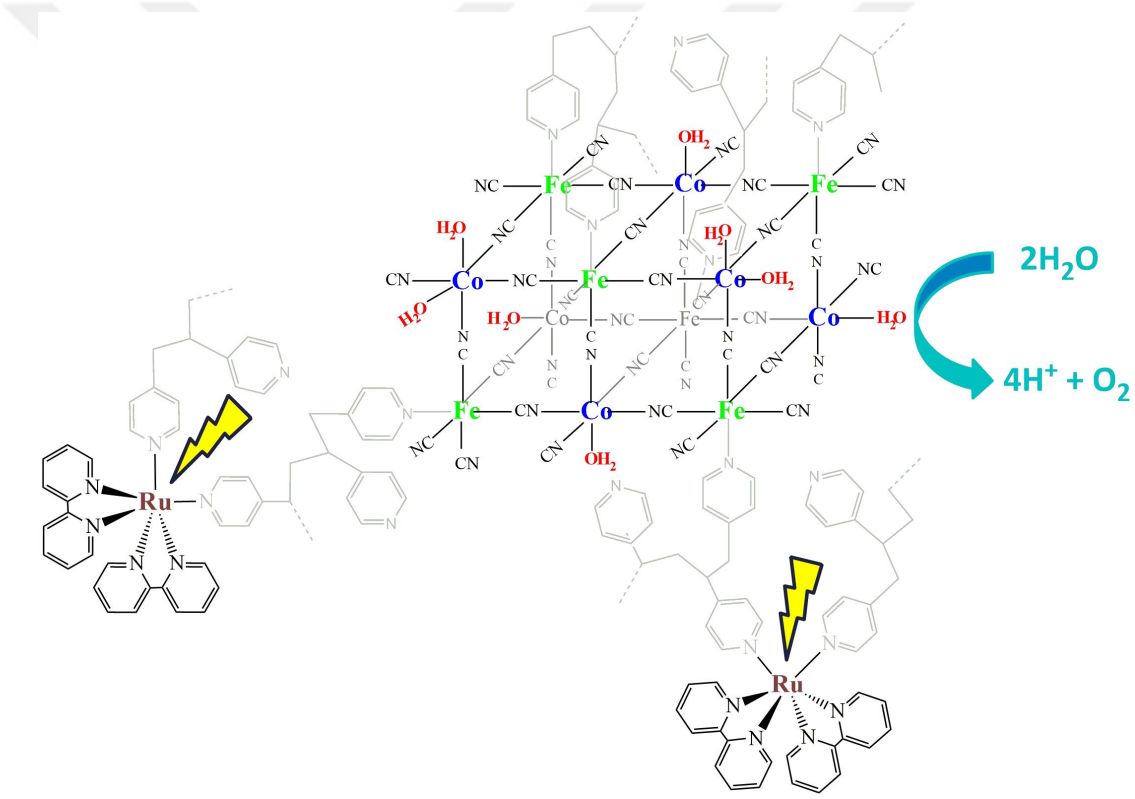

Figure 1.13: Proposed structure of the ruthenium chromophore and cobalt-based PBA dyad, incorporating poly(4-vinylpyridine).

In the second part of the study, a facile synthetic pathway using poly(4-vinylpyridine) as a polypyridyl platform is reported for the formation of cobalt-based metallopolymer (Figure 1.14). Electrochemical studies indicate that similar cobalt polypyridyl complexes act as an efficient H_2 evolution catalyst.[29],[34],[39],[40],[41] In particular, poly(4-vinylpyridine) is used as ligand since it is a commercially available polymer, and consequently a facile synthesis method is presented. Furthermore, since molecular complexes have a

tendency to disintegrate under drastic electrocatalytic and photocatalytic conditions, possible transformation of metallopolymer to cobalt particles was also investigated.[46],[49] Therefore, this study outlines a detailed electrochemical investigation of cobalt–polymer systems as well as their transformation to cobalt-based particles, which are active electrocatalysts for H_2 evolution.

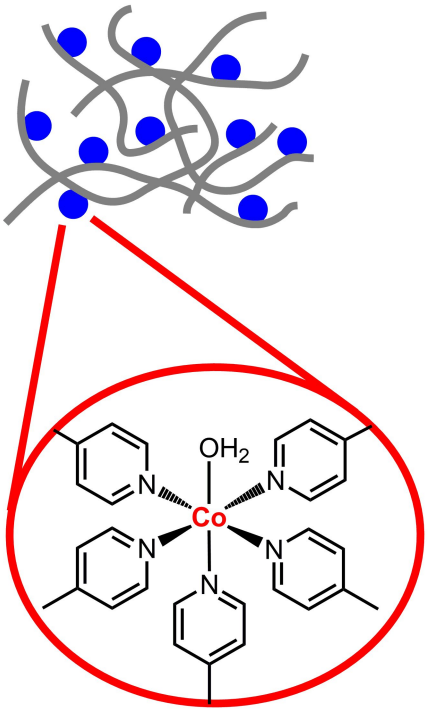

Figure 1.14: Proposed structure of cobalt- poly(4-vinylpyridine) catalyst.

Chapter 2

Experimental

Parts including 2.6 and 2.6.1 are based on the publication "Electrocatalytic hydrogen evolution with cobalt–poly(4-vinylpyridine) metallopolymers", Zeynep Kap; Emine Ülker; Satya Vijaya Kumar Nune; Ferdi Karadas, Journal of Applied Electrochemistry, 2018, 48 (2): 201-209. "Reprinted by permission from Springer Nature. Copyright 2018, Journal of Applied Electrochemistry.

2.1 Reagents and Materials

cis-Bis(2,2' - bipyridine)dichlororuthenium(II) hydrate (Acros Organics, 97%), poly(4-vinylpyridine) (Sigma-Aldrich, MW $\approx 60,000$ g/mol), $AgNO_3$ (Sigma-Aldrich, $\geq$ 99.0), $Na_2[Fe^{III}(CN)_5NO]\cdot 2H_2O$ (Alfa Aesar, 98%), NaOH (Sigma-Aldrich, 98-100.5%), and cobalt acetate tetrahydrate (Acros Organics, 98%) were used. All of the solvents were analytical grade and reagents received were used without any further processing. Millipore deionized water (resistivity: 18 mΩ cm) was used for all experiments that consists water.

2.2 Synthesis of [Ru-P4VP]

At room temperature, 700.0 mg (1.445 mmol) *cis-Bis*(2,2' - bipyridine)dichlororuthenium(II) hydrate and 490.9 mg (2.890 mmol) $AgNO_3$ were mixed in 100 mL methanol according to the literature with slight modifications.[56] After 1 h of vigorous stirring, precipitated layer of AgCl was filtered through celite filter and removed. $[Ru(bpy)_2(H_2O)_2](NO_3)_2$ filtrate was evaporated by rotary evaporator. $[Ru(bpy)_2(H_2O)_2](NO_3)_2$ was added to the solution of 6-fold molar excess of poly(4-vinylpyridine) which was dissolved in 200 mL 4:1 ethanol/water. The mixture was refluxed in dark for 48 h under constant stirring. Completion of the product was monitored by UV-Visible spectroscopy. Resulting solution was evaporated by rotary evaporator, dissolved in ethanol, precipitated by ethyl ether.[57] The precipitate was filtered and rinsed with cold water and ethyl ether. Throughout the thesis, the abbreviation [Ru–P4VP] is used for the $[Ru(bpy)_2(P4VP)_6]^{2+}$.

2.3 Synthesis of $Na_3[Fe^{II}(CN)_5NH_3]\cdot 3H_2O$

$Na_3[Fe^{II}(CN)_5NH_3]\cdot 3H_2O$ was synthesized according to the procedure in literature with slight modifications.[54],[58] 30 g of $Na_2[Fe^{III}(CN)_5NO]\cdot 2H_2O$ and 4 g NaOH were mixed in 120 mL of water under constant stirring. NaOH was used as excess sodium source to prevent a secondary reaction which would lead disodium salt, $Na_2NH_4Fe^{II}(CN)_5NH_3$.[58] The overall reaction is shown below.

$$Na_2Fe^{III}(CN)_5NO \cdot 2H_2O + 2NH_3 + NaOH \rightarrow Na_3Fe^{II}(CN)_5NH_3 \cdot 3H_2O + H_2O + N_2 \quad (2.1)$$

Throughout the experiment, temperature was kept below 10 °C. After obtaining homogenous solution, 25% (v/v) NH_4OH solution was added until saturation, by making sure the temperature is not exceeding 10 °C. Solution was stirred for 1 h, followed by the addition of cold methanol until yellow color wass obtained. After vacuum filtration, resulting precipitate was dried in vacuum oven for 4 days

at 25 °C. The product was recrystallized using a NH_4OH and CH_3OH solutions for two times to remove any unreacted precursor and by-product. Resulting yield was 45%. IR (cm^{-1}): 2031(s), 1625 (w), 1262(s).

2.4 Synthesis of [Ru-P4VP-Fe]

$Na_3[Fe^{II}(CN)_5NH_3]\cdot 3H_2O$ was used as Fe precursor. [Ru-P4VP] was dissolved in methanol and precursor was added to the solution according to 1:2 Ru/Fe stochiometric ratio. Solution was kept in dark under constant stirring for 5 days. Cold [Ru-P4VP-Fe] solution was centrifuged with water several times and liquid phase was discarded. Complex was dried in vacuum desiccator after washing with acetone. Throughout this thesis, the abbreviation [Ru-P4VP-Fe] is used for the $[Ru(bpy)_2(P4VP)_6]$-$Fe(CN)_5$ assembly.

2.5 Synthesis of [Ru-P4VP-CoFe]

Cobalt(II) acetate tetrahydrate was used as Co precursor. [Ru-P4VP-Fe] was dissolved in 1:1 (v/v) acetonitrile/water solution and Co precursor was added. Co precursor was added according to the 3:2 Co/Fe stochiometric ratio. Solution was kept in dark under constant stirring for 2 days following evaporation by rotary evaporator. Throughout this thesis, the abbreviation [Ru-P4VP-CoFe] is used for the $[Ru(bpy)_2(P4VP)_6]$-$CoFe(CN)_5$ assembly.

2.6 Synthesis of [Co-P4VP]

Cobalt acetate tetrahydrate ($CoAc_2$) and poly(4-vinylpyridine) (P4VP) were mixed in a 1:1 H_2O/MeCN (v/v) mixture. $CoAc_2$ and P4VP were added according to stoichiometric ratio of 1:5 Co/pyridine to ensure that each cobalt

ion is surrounded by an average number of five pyridine groups and one solvent molecule. Throughout the thesis, the abbreviation [Co–P4VP] will be used for the metallopolymer.

2.6.1 Formation of [Co-coat@FTO]

A solution of [Co–P4VP] (1 mM) in a 1:1 H_2O/MeCN mixture containing 3 mM of AcOH and 0.1 M of KNO_3 under nitrogen was electrolyzed at -1.5 V (vs. $Fc^{+/0}$) for 2 h using fluorine-doped tin oxide (FTO) (area: 1 cm^2) as the working electrode. The electrode was washed several times with an H_2O/MeCN mixture after coating. Cobalt particle coated FTO is abbreviated as [Co-coat@FTO] throughout the thesis.

2.7 Instrumentation

2.7.1 Fourier Transform Infrared Spectroscopy

Fourier transform infrared spectra (FTIR) were recorded by Bruker Alpha Platinum-ATR Spectrometer model. The spectra were recorded in transmission mode by 64 scans in wavenumber range of 400-4000 cm^{-1}.

2.7.2 Ultraviolet-Visible Spectroscopy

The UV-Vis absorption spectra were recorded by using Cary 100 Bio UV-Vis Spectrometer in the 200-800 nm region with a scan rate 600 nm/min.

2.7.3 X-Ray Photoelectron Spectroscopy

XPS analysis was performed using Thermo Scientific K-Alpha X-Ray Photoelectron Spectrometer system with an AlK_{α} microfocused monochromator source operating at 400 mm spot size and $h\gamma = 14.866$ eV accompanied by a flood gun for charge neutralization, 200 eV for survey scan and 30 eV for individual scans.

2.7.4 X-Ray Powder Diffraction

XRD measurement was conducted by using a Pananalytical X'PertPro Multipurpose X-Ray Diffractometer (MPD) with CuK_{α} X-Ray Radiation ($\lambda = 1.5418$). The diffraction patterns were recorded in the 2θ diffraction angle in 10-70° range with 0.05 step size.

2.7.5 Scanning Electron Microscopy and Energy-Dispersive X-Ray Spectroscopy

FEI-Quanta 200 FEG ESEM was used for SEM and EDX analysis. For SEM imaging, 5 kV beam voltage was used and EDX analysis was operated at 30 kV beam voltage. Each EDX analysis was reported by taking mean value from multiple measurements of different spots.

2.7.6 Photocatalytic Studies

The oxygen amount was measured with GC (Agilent 7820A, Molesieve GC column (30 m × 0.53 mm × 25 μm)) thermostatted at 40°C which was equipped with a TCD detector thermostatted at 100°C (Ar as carrier gas). Oxygen evolution was calibrated with pressure transducer (Omega PXM409-002BAUSBH). The solar light simulator (Sciencetech, SLB-300B, 300 W Xe lamp, AM 1.5 global

filter) was calibrated to 1 sun (100 mW/cm^2). Experimental setup is shown in Figure 2.1.

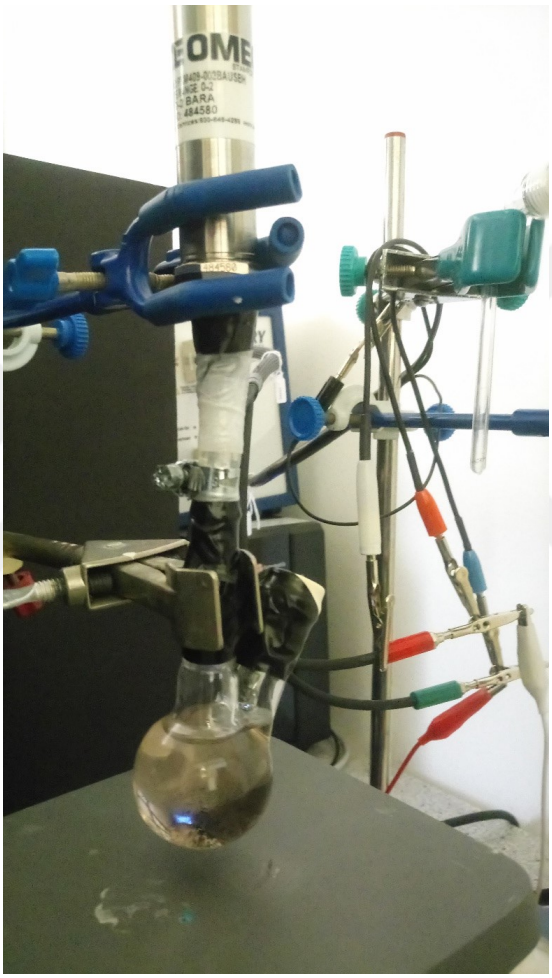

Figure 2.1: Photocatalytic setup consisting a two-neck round-bottom flask connected to pressure transducer. One neck is covered with septa and used for N_2 purge and GC measurements.

For each photocatalytic measurement, 10 mL phosphate pH 7.0 buffer was used, and 25 mg sodium persulfate was added as the sacrifial electron acceptor. All measurements were done under constant stirring, and flask were covered with aluminum foil until the light was on. Pressure transducer was connected to two-neck round-bottom flask with 41.4 mL volume in which one neck was covered with septa. Before light illumination, solution was purged with N_2 for 30 min, and two

needles were used for N_2 in and out. When plateau was observed on pressure, 100 μL from the headspace of the cell was injected with gas-tight syringe into a gas chromatograph as an initial measurement. Pressure was allowed to reach plateau, and followingly light was on for 1 h. After 1 h of light illumination, light was off, and gas phase was analyzed by GC. During the process, pressure change was recorded versus time.

Blank measurement was also taken according to the same procedure. Solution was consisted of 10 mL phosphate pH 7.0 buffer, and 25 mg sodium persulfate.

TOF and TON were derived by using the data obtained from GC. O_2 to N_2 area ratio were calculated, and the value was multiplied with the headspace volume of the cell (31.4 mL), then divided by injection volume of the gas tight syringe (100 μL) to obtain total O_2 amount in the cell. Subsequently, total O_2 amount of blank measurement and initial measurement were subtracted from the final experimental value.

Galan-Mascaros et al. reported that the TOF obtained was 4.5 x 10^{-4} s^{-1}, and it was used as a reference value.[52] 5 mg $[Ru(bpy)_3]^{2+}$, 5 mg Co-Fe PBA, and 25 mg sodium persulfate were dissolved in 10 mL phosphate pH 7.0 buffer, and photocatalytic experiment was conducted according to the above procedure. After necessary subtractions, total amount of O_2 obtained was multiplied with a constant which will give TOF of 4.5 x 10^{-4} s^{-1} to obtain mole of O_2 produced. Mole of O_2 was used to calculate TOF, and equation is as follows:

$$\text{mole of } O_2 \text{ produced} = \text{total } O_2 \text{ amount} \times \text{constant} \tag{2.2}$$

$$\text{TOF} = \frac{\text{mole of } O_2 \text{ produced}}{\text{mole of catalyst} \times \text{time}} \tag{2.3}$$

Constant derived according to the calculations were then used in [Ru-P4VP-CoFe] measurements to obtain mole of O_2, TOF, and TON values. For mole of catalyst value, it is assumed that all Co sides are active for water oxidation. TON

equation is as follows:

$$\text{TON} = \text{TOF} \times \text{time} \tag{2.4}$$

After each photocatalytic experiment of [Ru-P4VP-CoFe] and $[Ru(bpy)_3]^{2+}$ and Co-Fe PBA systems, samples were kept in fridge for 1 day and re-used with the addition of 25 mg sodium persulfate.

2.7.7 Gas Chromatography

The gas generated during the electrolysis was analyzed with an Agilent 7820A GC equipped with a Molesieve GC column (30 m $\times$ 0.53 mm $\times$ 25 μm) thermostatted at 40°C and a TCD detector thermostatted at 100°C for the detection of H_2. Ar was used as carrier gas. To avoid cross-contamination, prior to each experiment, the electrochemical cell was purged with N_2 for 20 min. Then, 100 μL aliquots of gas were collected from the headspace of the electrochemical cell over 10 min intervals with a gas-tight Hamilton syringe. The retention time of H_2 was recorded as 0.77 min.

2.7.8 Electrocatalytic Studies

Electrochemical experiments were performed at room temperature using a Gamry Instruments Interface 1000 Potentiostat/Galvanostat. A conventional three-electrode electrochemical cell was used with a glassy carbon disc electrode (GCE) (area = 0.071 cm^2) as the working electrode and a Pt wire as the counter electrode. The working electrode was cleaned after each measurement by polishing with an alumina (0.05-μ diameter) suspension followed by sonication with water. The pseudo-reference electrode was a silver wire immersed in 1:1 H_2O/MeCN (v/v) mixture with 0.1 M KNO_3, which was separated from the solution by a glass frit. Ferrocene was used as an internal standard and all potentials were

referenced versus the ferrocenium/ferrocene couple ($Fc^{+/0}$) (0.64 V vs. SHE). AcOH was used as the proton source in the hydrogen evolution experiments. All experiments were carried out under a nitrogen atmosphere.

2.7.8.1 Bulk Water Electrolysis

The bulk electrolysis experiment was performed in a H_2O/MeCN (1:1 v/v) mixture with 0.1 M of KNO_3 containing 60 mM of AcOH at -1.5 V (vs. $Fc^{+/0}$) for 2 h. A Pt mesh counter electrode was separated from the rest of the solution by a glass frit. [Co-coat@FTO] was used as the working electrode.

Chapter 3

Results and Discussion

In this chapter, parts 3.1.2 and 3.2.3 are based on the publication "Electrocatalytic hydrogen evolution with cobalt–poly(4-vinylpyridine) metallopolymers", Zeynep Kap; Emine Ülker; Satya Vijaya Kumar Nune; Ferdi Karadas, Journal of Applied Electrochemistry, 2018, 48 (2): 201-209. "Reprinted by permission from Springer Nature. Copyright 2018, Journal of Applied Electrochemistry.

3.1 Structural Characterization

3.1.1 [Ru-P4VP-CoFe] for Light-Driven Water Oxidation

3.1.1.1 Fourier Transform Infrared Spectroscopy

According to the Infrared studies following conclusions were made;

i) CN stretching mode typically exhibits a sharp absorption peak which is observed in 2000-2200 cm^{-1} band, and a possible shift in this characteristic range is the major confirmation for CN linkage.[59],[60] CN stretches observed at 2034 cm^{-1} and 2103 cm^{-1} for [Ru-P4VP-Fe] indicates that Fe^{2+} is covalently linked

with pyridyl group of [Ru-P4VP].[54] The relatively small peak at 2103 cm^{-1} is a result of the partial oxidation of the iron sites to Fe^{3+} (Figure 3.1).[54]

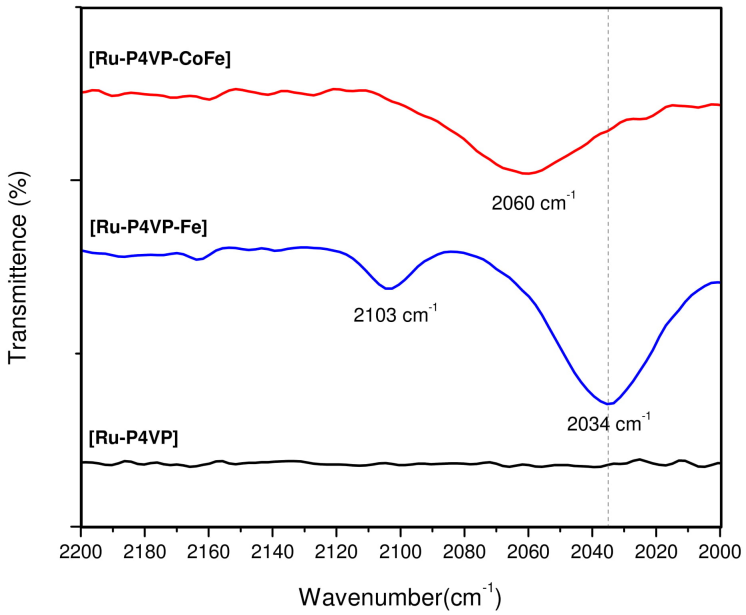

Figure 3.1: FTIR spectra of [Ru-P4VP], [Ru-P4VP-Fe], and [Ru-P4VP-CoFe].

ii) Slight blue shift to 2034 cm^{-1} compared to Fe precursor (2031 cm^{-1}) suggests that there is no free iron pentacyanoferrate which is not linked with pyridyl rings (Figure 3.1).[54] The increase in the frequency is due to π-accepting ability of pyridine of P4VP which results in less back electron donation from d_π orbital of iron to π^* orbital of cyanide.

iii) With the addition of Co^{2+}, a prominent blue shift is observed at 2060 cm^{-1} for [Ru-P4VP-Fe-Co] which is a clear demonstration of Fe-CN-Co linear binding mode, and therefore Co-Fe PBA synthesis (Figure 3.1).[53] As a result of Co ion addition, the structure became more electron deficient, and consequently electron donation from σ^* orbital of cyanide increases, thus CN stretch is observed at a higher frequency. Broader peak observed in [Ru-P4VP-CoFe] compared to [Ru-P4VP-Fe] was attributed to partial oxidized Fe(III) sites bound to Co(II).

iv) [Ru-P4VP] has stretches at 1417 cm^{-1} and 1597 cm^{-1} which are attributed to C=C_{ring} and C=N_{ring} of pyridyl rings (Figure 3.2).[54],[61]

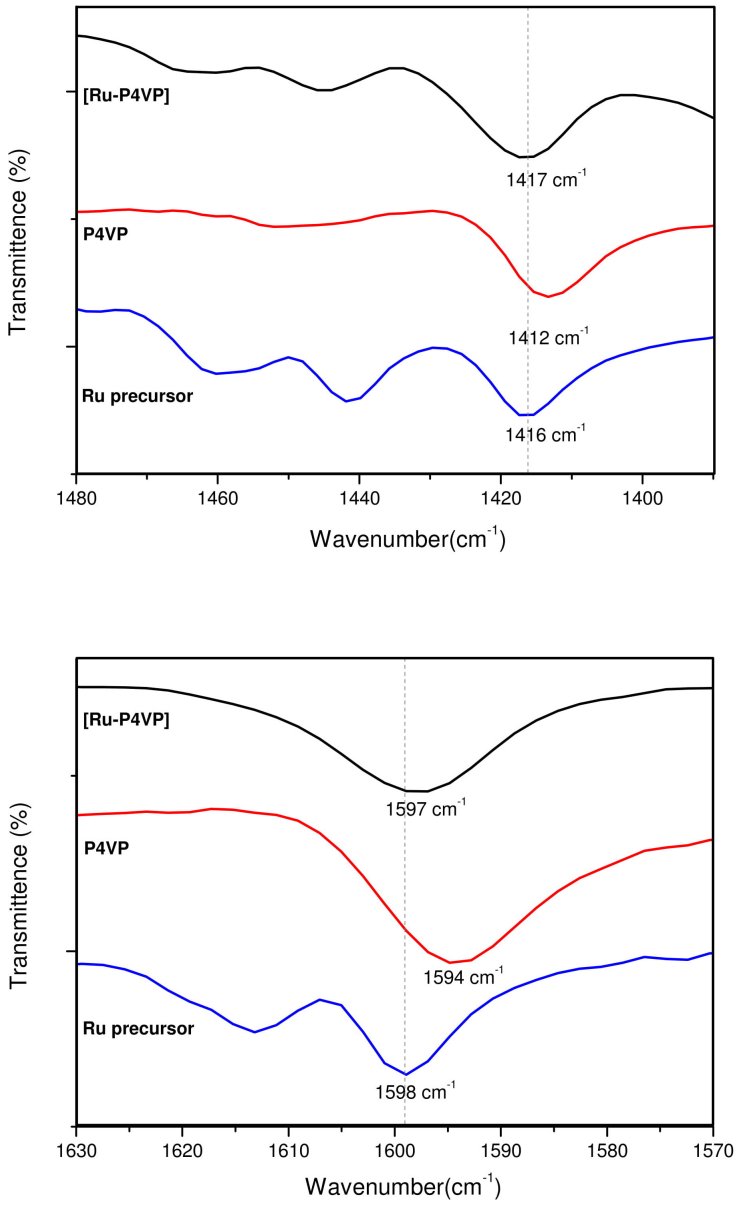

Figure 3.2: FTIR spectra of Ru precursor, P4VP, and [Ru-P4VP].

3.1.1.2 Ultraviolet-Visible Spectroscopy

Ru precursor shows two main bands which are assigned to the metal-to-ligand charge transfer (MLCT) at 526 nm and ligand centered π-π^* (LC) at 283 nm respectively (Figure 3.3). In all cases, the blue shift to 450 nm (with shoulder at 435 nm) verifies the complex formation which corresponds to typical bands for *tris*-Ru(II) pyridine complexes.[62],[63],[64] With the addition of Fe and Co precursors, MLCT character of the [Ru-P4VP] showed similar results with the [Ru-P4VP-Fe] and [Ru-P4VP-CoFe] complexes (Figure 3.4).

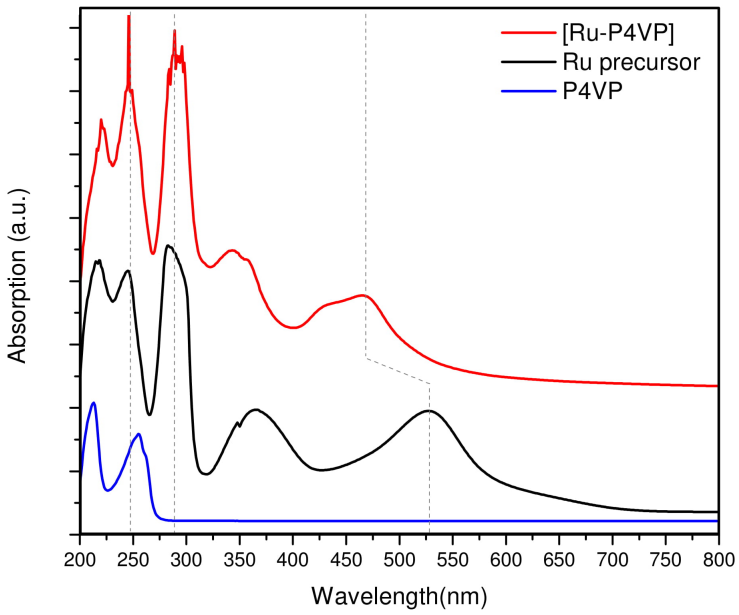

Figure 3.3: UV-Vis spectra of P4VP (blue line), Ru precursor (black line), and [Ru-P4VP] (red line).

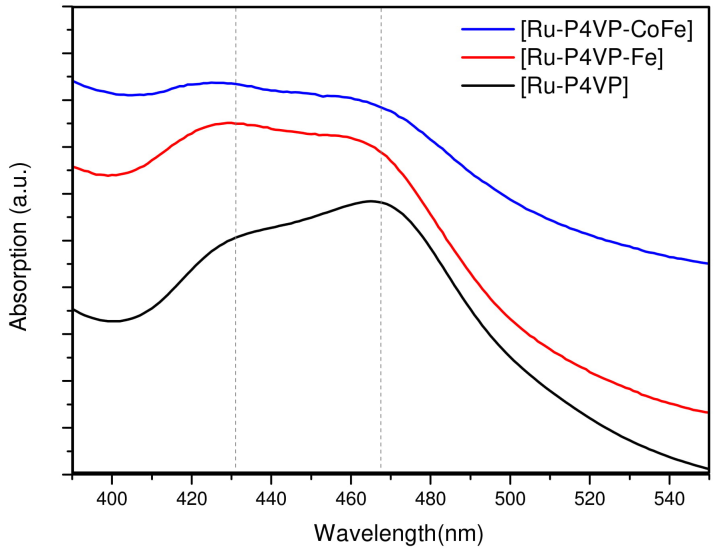

Figure 3.4: UV-Vis spectra of [Ru-P4VP] (black line), [Ru-P4VP-Fe] (red line), and [Ru-P4VP-CoFe] (blue line).

3.1.1.3 X-Ray Photoelectron Spectroscopy

As it is shown in (Figure 3.5), Ru $3d_{5/2}$ and $3d_{3/2}$ signals of [Ru-P4VP] were observed at 280.21 eV and 284.96 eV, respectively, where Ru $3d_{5/2}$ signal of Ru precursor is observed at a slightly lower binding energy (280.75 eV). This change in binding energy is attributed to the replacement of chloride groups with pyridyl ones leading a decrease in electron density of ruthenium. Besides, the Ru 3d signals in [Ru-P4VP], [Ru-P4VP-Fe], and [Ru-P4VP-CoFe] samples are similar in chemical nature, and there is no significant change in oxidation state. The slight change in [Ru-P4VP-Fe] to 280.98 eV and 284.96 eV for Ru $3d_{5/2}$ and Ru $3d_{3/2}$, respectively, is attributed to partial oxidation of $Fe^{3+/2+}$. Two shoulder bands are observed at $\approx$ 711.51 eV and $\approx$ 725.21 eV in Fe 2p signals of [Ru-P4VP-Fe] are also due to of Fe^{2+} to Fe^{3+} ions in $Fe(CN)_5$ fragments (Figure 3.6). Such oxidation is commonly observed in pentacyanoferrate chemistry, and results are in good agreement with IR spectra, which reveals a shoulder band in the

cyanide region at 2103 cm^{-1} for [Ru-P4VP-Fe].

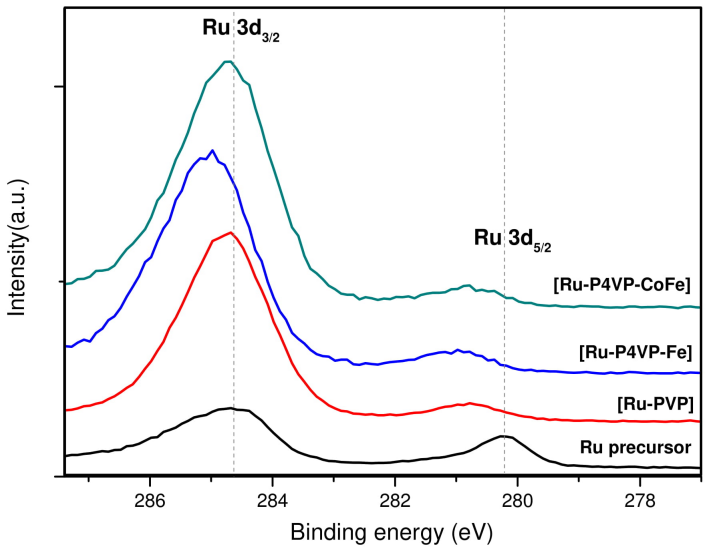

Figure 3.5: XPS spectra of Ru 3d signals of Ru precursor, [Ru-P4VP], [Ru-P4VP-Fe], and [Ru-P4VP-CoFe].

Fe 2p signals for [Ru-P4VP-Fe] are observed at around 708.69 eV and 722.69 eV which are assigned as Fe $2p_{3/2}$ and Fe $2p_{1/2}$, respectively (Figure 3.6). Signals corresponded well with Fe precursor showing that they are in similar chemical environment. Broad peaks compared to precursor were observed for both [Ru-P4VP-Fe] and [Ru-P4VP-CoFe] samples due to partial oxidation of Fe^{2+} to Fe^{3+} ions in $Fe(CN)_5$ fragments. For [Ru-P4VP-CoFe], Fe 2p signal was observed with a lower intensity and showed a noisy response. Although Co-$Fe(CN)_5$ bound to PV4P was proved with IR spectroscopy, reason for such behavior cannot be found.

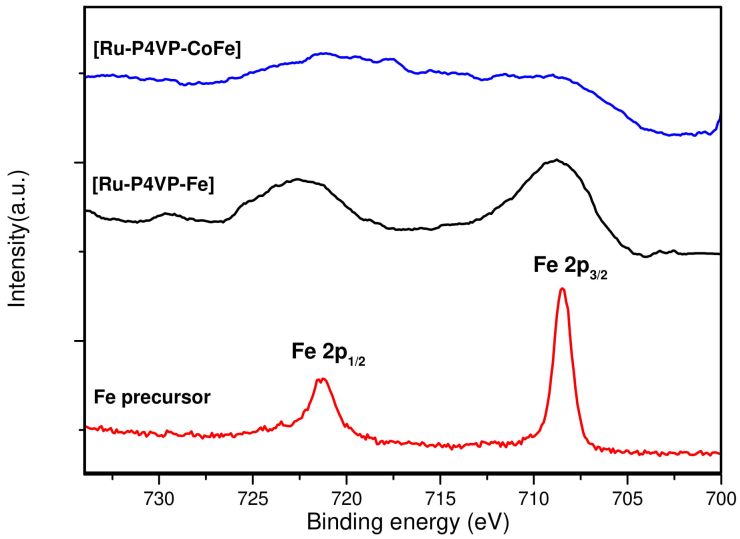

Figure 3.6: XPS spectra of Fe 2p signals of Fe precursor, [Ru-P4VP-Fe], and [Ru-P4VP-CoFe].

N 1s signals indicate that all samples exhibit similar profiles (Figure 3.7). A slight decrease in binding energy of [Ru-P4VP] compared to Ru precursor is attributed to an increase in the electron density of pyridyl ring because of π back-bonding interaction between ruthenium and pyridyl groups of P4VP. Similar response is also observed for [Ru-P4VP-Fe] and [Ru-P4VP-CoFe].

Co $2p_{3/2}$ and $2p_{1/2}$ signals of the Co precursor showed peaks at 781.09 eV and 796.96 eV, respectively, and compared to [Ru-P4VP-CoFe] signals (781.01 eV and 796.54 eV, respectively), similar responses were obtained which proves the Co^{2+} form (Figure 3.8).[65] Furthermore, [Ru-P4VP-CoFe] showed distinctive satellite signals at binding energies approximately 5 eV higher than principal signals.

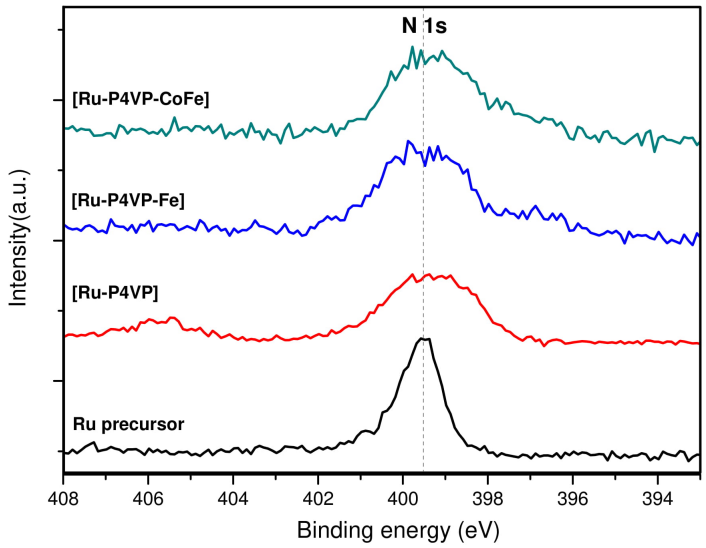

Figure 3.7: XPS spectra of N 1s signals of Ru precursor, [Ru-P4VP], [Ru-P4VP-Fe], and [Ru-P4VP-CoFe].

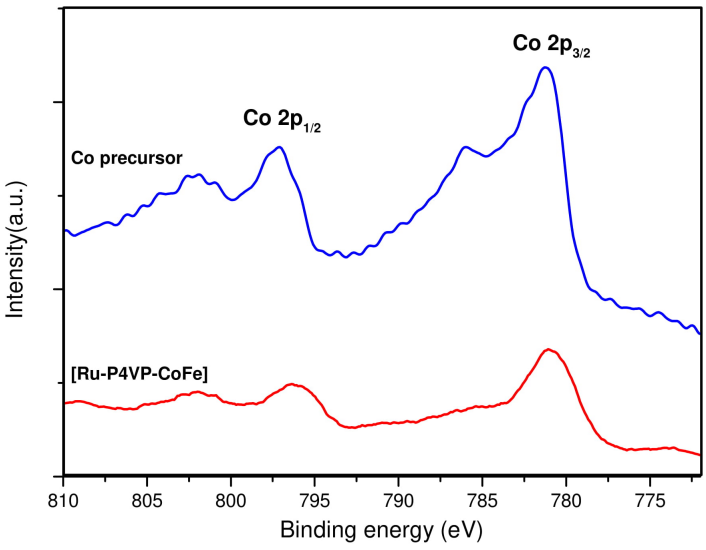

Figure 3.8: XPS spectra of Co 2p signals of [Ru-P4VP-CoFe], and Co precursor.

3.1.1.4 X-Ray Powder Diffraction

XRD analysis in grazing incidence mode was conducted on [Ru-P4VP-CoFe] powder to establish the amorph structure of the assembly. In the XRD pattern, no crystalline structure is observed, except some of the characteristic peaks of Prussian Blue (Figure 3.9). Structure analysis is also performed with SEM to support XRD.

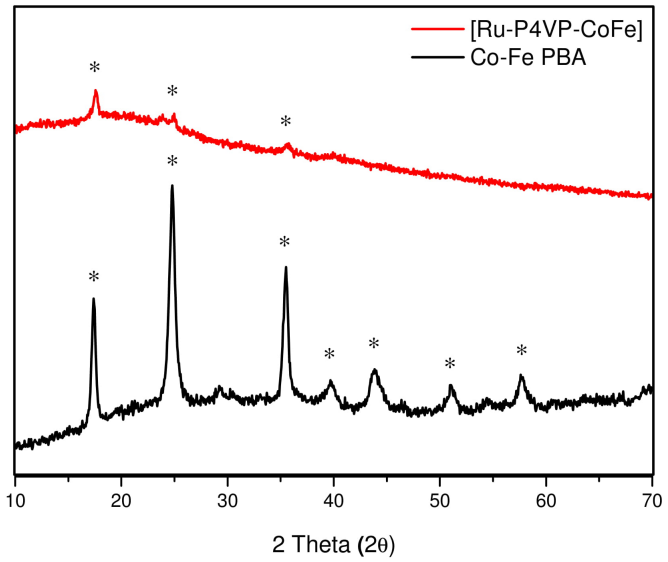

Figure 3.9: GI-XRD patterns of [Ru-P4VP-CoFe] (red line), and Co-Fe PBA (black line). The peaks that belong to Prussian blue are marked with asterisk (*).

3.1.1.5 Scanning Electron Microscopy and Energy-dispersive X-Ray Spectroscopy

According to EDX results, [Ru-P4VP-CoFe] was found as $Na_{0.97}Co_{2.86}[Fe(CN)_5]_{2.13}$-$[P4VP]_6$-$[Ru(bpy)_2]Cl_{2.89}$. Atomic ratios were calculated by averaging 3 different sample measurements of different points (Table 3.1). EDX spectrum of [Ru-P4VP-CoFe] is shown in (Figure 3.10).

It should be noted that, all P4VP is estimated to react with Ru precursor[56],[57], therefore repeating unit of ruthenium bound to pyridyl monomer is six. Overall, as it was demonstrated in Figure 3.10, $Co[Fe(CN)_5]$ unit is connected with one pyridyl group of the P4VP where two pyridyls are coordinated with one ruthenium ion.

Table 3.1: Atomic percentage values of the elements in [Ru-P4VP-CoFe]

# of EDX Analysis	**Atomic % by Ru***	**Atomic % by Cl***	**Atomic % by Na***	**Atomic % by Fe***	**Atomic % by Co***
1	1	3.17	1.30	2.56	3.41
2	1	3.48	0.88	1.87	2.88
3	1	2.03	0.75	1.97	2.29
Average Number	**1**	**2.89**	**0.97**	**2.13**	**2.86**

*Values were divided to atomic percentage value of Ru content.

Results shows the lack of homogeneity of the assembly where the atomic ratio of Ru to Fe atoms varies from 1.87 to 2.56. A possible reason is the amorphous structure that has a polymer chain surrounding the Ru, Fe, and Co metals from various positions. SEM images also support the amorphous structure of the assembly (Figure 3.11). Approximately 50 nm sized Prussian Blue particles were observed that are coordinated with the bulk material, and this result is in good agreement with XRD findings. Lack of homogeneity of Co/Fe ratio is attributed to two limiting compositions of PBA; $NaCo[Fe(CN)_5]$ and $Co_3[Fe(CN)_5]$ where Co/Fe ratio varies between 1:1 to 3:2, respectively.[66] Cl ions existence were attributed to free Cl ions compensating positively charged $[Ru(bpy)_2(P4VP)_6]^{2+}$.

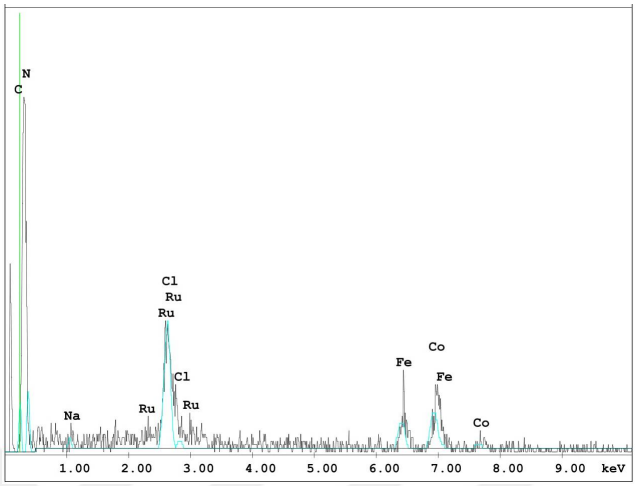

Figure 3.10: EDX spectrum of [Ru-P4VP-CoFe].

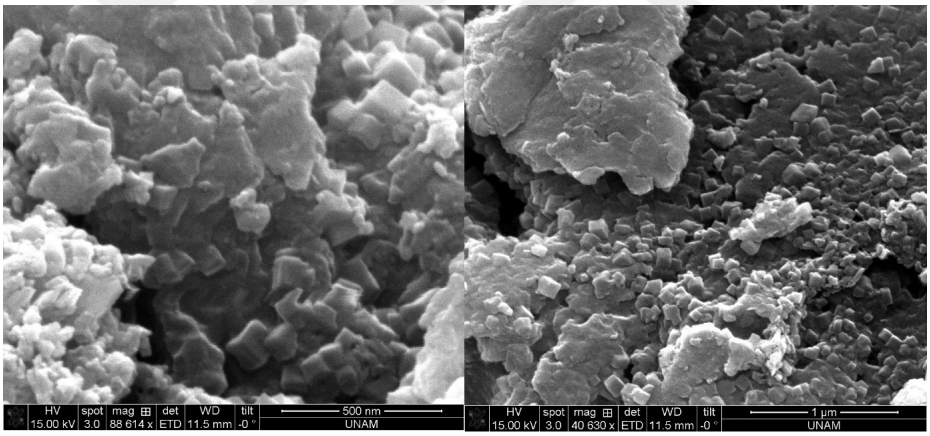

Figure 3.11: SEM images of [Ru-P4VP-CoFe].

3.1.2 [Co-P4VP] for Water Reduction

3.1.2.1 Ultraviolet-Visible Spectroscopy

UV-Vis Spectroscopy was performed on [Co-P4VP] systems with different metal to ligand ratios, 1:5, 1:10, and 1:50 to analyze coordination environment of the assembly. Absorption spectra of these derivatives showed similar results (Figure 3.12). A broad band at 506 nm ($\epsilon = 12 \times 10^3$ M^{-1} cm^{-1} for [Co-P4VP] (1:5)) with a shoulder at 463 nm that is attributed to a metal-to-ligand charge transfer (MLCT) transition. This band is similar to some of the previously reported

Co(II) molecular systems.[67]

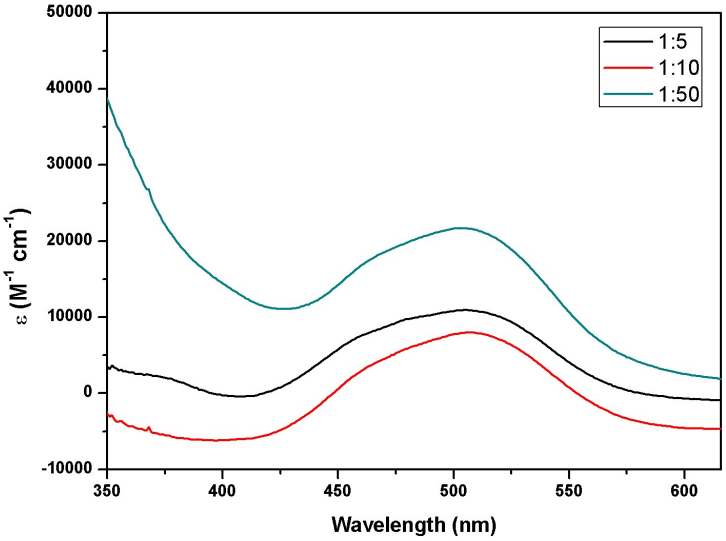

Figure 3.12: Absorption spectra of [Co-P4VP] systems with different metal to ligand ratio, 1:5 (red line), 1:10 (blue line), and 1:50 (green line).

3.1.2.2 X-Ray Photoelectron Spectroscopy

N 1s peak of XPS for P4VP positioned at 399 eV showed a visible shift to a slightly higher binding energy in the resulting compound indicating a variation in the charge due to the formation Co-N bonds (Figure 3.13).[68]

Figure 3.14 depicts the XPS spectra of Co 2p signals of the Co particles coated onto the FTO, Co(II) precursor, and [Co-P4VP]. Co $2p_{3/2}$ and Co $2p_{1/2}$ signals of [Co-P4VP] were observed as broad peaks at 782.38 eV and 798.08 eV, respectively, with FWHM of approximately 2 – 2.5 eV in [Co-P4VP], which corresponds well with the Co(II) precursor data (782.28 eV and 798.38 eV, respectively), indicating the absence of a significant change in the oxidation state.[65] Moreover, distinctive and scalable satellite signals were also observed at binding energies 4 – 5 eV higher than the principal signals. However, Co 2p signals of the [Co-coat@FTO] show only a mild shift. Co $2p_{3/2}$ and Co $2p_{1/2}$ signals were observed as strong intense

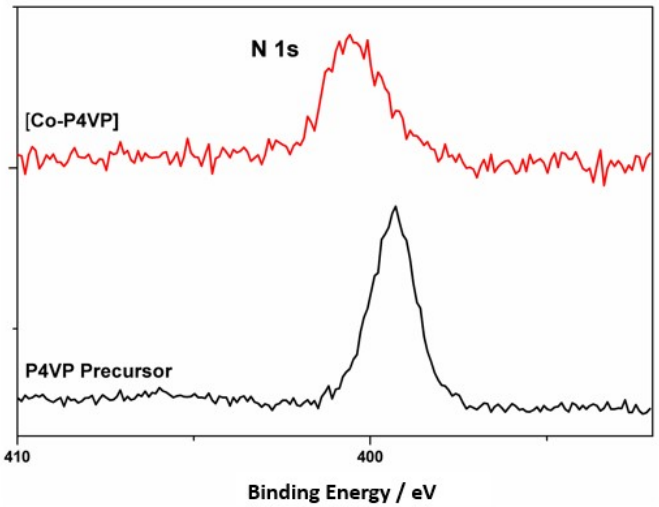

Figure 3.13: XPS spectra of N 1s signals of P4VP precursor and [Co-P4VP].

peaks at 780 eV and 795 eV, respectively, with FWHM of approximately 2.5-3 eV with insignificant or negligible satellite signals. The mild shift in the position of the principle signals and insignificant satellite signals infer the presence of a mixture of oxidation states.

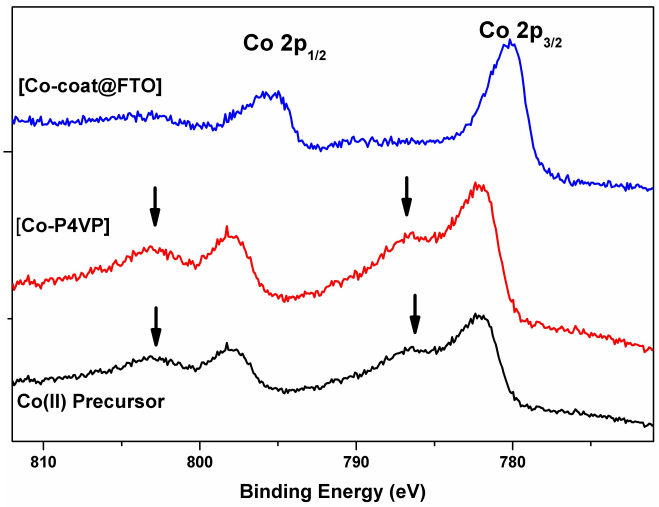

Figure 3.14: XPS spectra of Co 2p signals of Co(II) precursor, [Co-P4VP], and [Co-coat@FTO]. Black arrows represent satellite signals.

Similar studies of N 1s and C 1s signals (Figure 3.15) revealed that the Co particles coated onto the FTO electrode exhibit a different chemical nature from

[Co-P4VP]. N 1s and C 1s signals of the coating deposited on the FTO corresponds well with the P4VP precursor, indicating no evident decomposition in the pyridine ring or the P4VP chains.

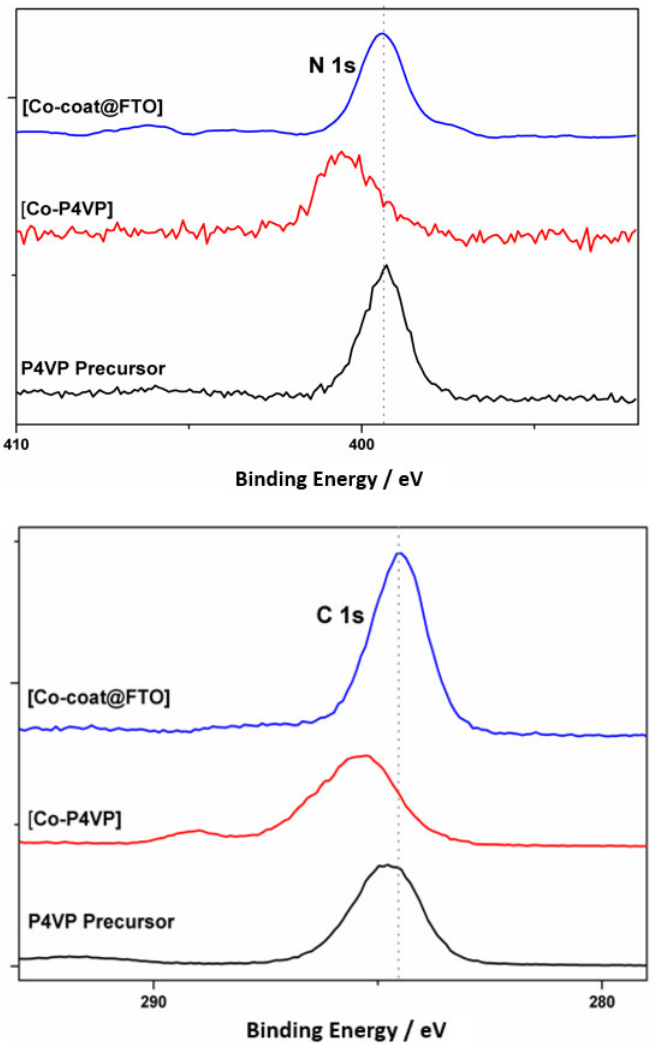

Figure 3.15: XPS spectra of N 1s signal and C 1s signals of the P4VP precursor, [Co-P4VP], and the [Co-coat@FTO].

3.1.2.3 Scanning Electron Microscopy

SEM images of the [Co-coat@FTO] (Figure 3.16) exhibit a continuous film of particles, which is in good agreement with the XPS analysis findings.

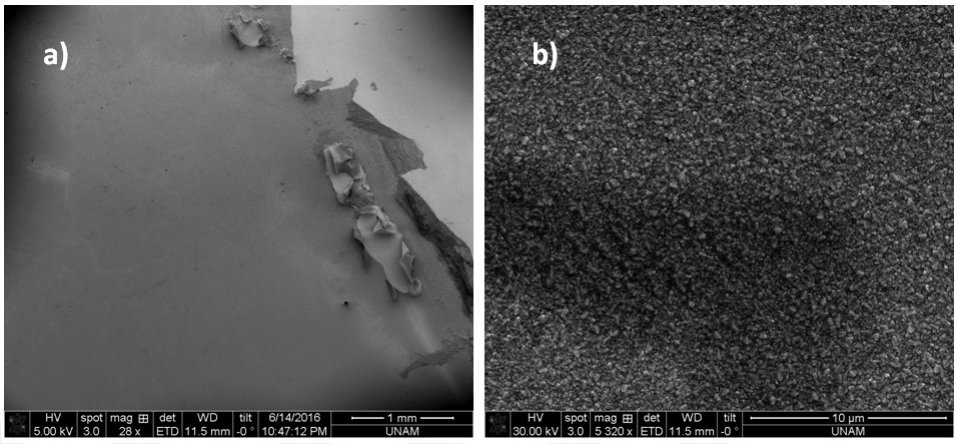

Figure 3.16: SEM images of the [Co-coat@FTO].

3.2 Catalytic Performance

3.2.1 [Ru-P4VP-CoFe] for Light-Driven Water Oxidation

Photocatalytic studies on [Ru-P4VP-CoFe] were performed using a suspension of powder sample in the presence of $Na_2S_2O_8$ as a sacrificial electron acceptor, at pH 7. Photocatalytic experiments were also performed with a previously studied Co-Fe PBA in the presence of $[Ru(bpy)_3]^{2+}$ / $S_2O_8{}^{2-}$ couple for comparison under same conditions.[52] In both experiments, the quantity of O_2 in the gas-tight set-up was measured before and after with gas chromatography. Blank measurement was also taken under same conditions except the addition of catalyst or chromophore.

The experiment for [Ru-P4VP-CoFe] was performed with the same batch for six cycles, and $[Ru(bpy)_3]^{2+}$ and Co-Fe PBA system was re-used up to three cycles. The $[Ru(bpy)_3]^{2+}$ and Co-Fe PBA curve yields a turnover frequency of 4.5 $\times$ 10^{-4} s^{-1}, which is in good agreement with the study reported.[52] The catalytic activity of $[Ru(bpy)_3]^{2+}$ and Co-Fe PBA system decreased gradually in following three cycles. In the final cycle, mole of O_2 produced reached to the value of blank measurement which is attributed to the decomposition of $[Ru(bpy)_3]^{2+}$ complex under photocatalytic conditions.[52] [Ru-P4VP-CoFe], however, maintained its

catalytic activity for six cycles. Catalytic activity is found slightly higher than that of $[Ru(bpy)_3]^{2+}$ and Co-Fe PBA system, and achieved a TOF of 5.6×10^{-4} s^{-1} in the first cycle (Figure 3.17).

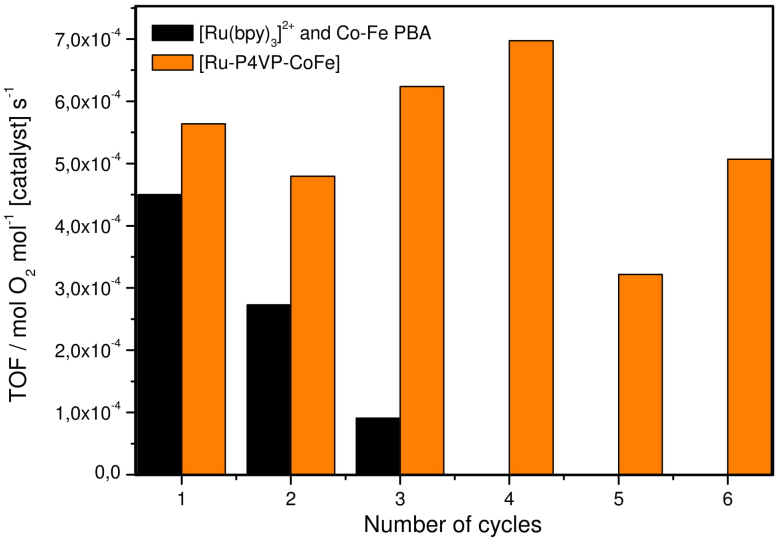

Figure 3.17: TOF vs. Number of cycles comparison of [Ru-P4VP-CoFe] (orange) and $[Ru(bpy)_3]^{2+}$ and Co-Fe PBA system (black). Each cycle duration is 1h.

TON of 11 is obtained after six cycles under total of 6 h light illumination where $[Ru(bpy)_3]^{2+}$ and Co-Fe PBA system had a TON of 2 after three cycles in 3 h period (Figure 3.18). Results shows that, ruthenium complex in [Ru-P4VP-CoFe] serves as a chromophore similar to $[Ru(bpy)_3]^{2+}$, and coupling it with a heterogeneous catalyst enhances its stability.

Comparison of TOF and TON values of proposed dyad with multi-component analogue suggest that more than 5-fold enhancement on activity is achieved. The higher activity of the assembly is attributed to its stability which is interrogated in detail by characterization studies performed on the post-catalytic sample.

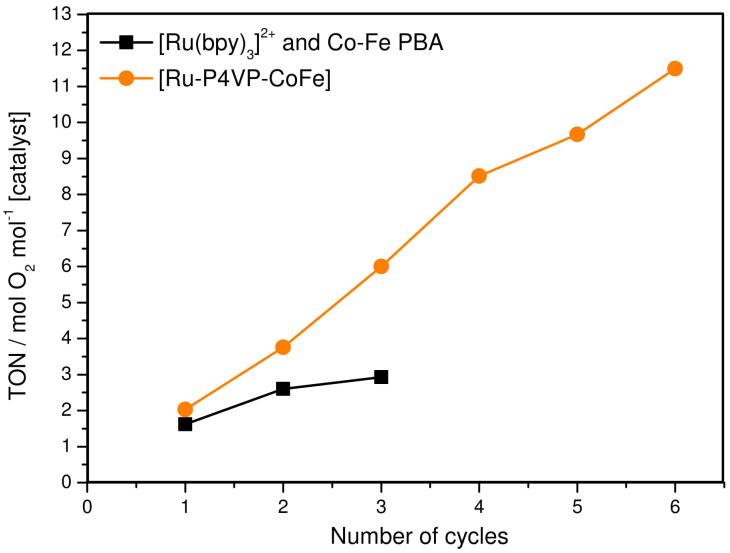

Figure 3.18: TON vs. Number of cycles comparison of [Ru-P4VP-CoFe] (orange circles) and $[Ru(bpy)_3]^{2+}$ and Co-Fe PBA system (black squares).

The XPS comparison of Co 2p and O 1s binding energies in the pristine and post-catalytic samples were performed to investigate the stability of [Ru-P4VP-CoFe]. Spectra of Co 2p bands exhibit similar Co $2p_{3/2}$, Co $2p_{1/2}$, and satellite bands. Moreover, lack of peaks below 780 eV rules out the decomposition of Co-Fe PBA to a possible catalytically active oxide species (Figure 3.19).[55] XPS of O 1s region was conducted to confirm that there is no decomposition of the metal coordinated clusters which might lead RuO_2. Result clearly shows that there is no oxide-based species which typically have lower binding energies than 530 eV, and peaks observed around 531 eV are only due to surface-adsorbed oxygen (Figure 3.20).[54] Therefore, after six cycles of re-using, dyad retains its structure, preserves its activity, and does not show any photo-decomposition character.

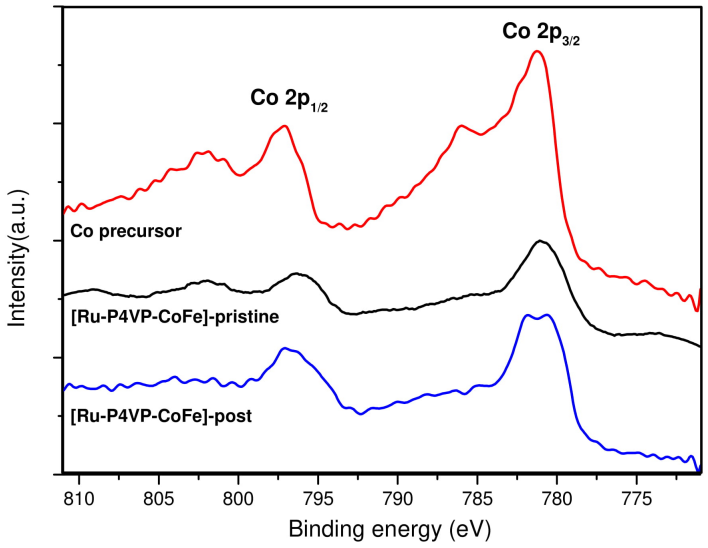

Figure 3.19: XPS spectra of Co 2p signals of [Ru-P4VP-CoFe] after six catalytic cycle, [Ru-P4VP-CoFe], and Co precursor.

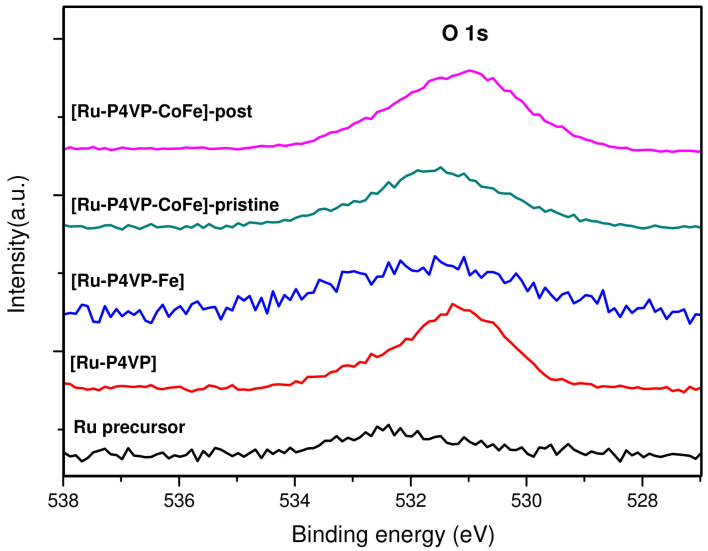

Figure 3.20: XPS spectra of O 1s signals of Ru precursor, [Ru-P4VP], [Ru-P4VP-Fe], [Ru-P4VP-CoFe], and [Ru-P4VP-CoFe] after six catalytic cycle.

Infrared study was also conducted to confirm stability of [Ru-P4VP-CoFe] after catalytic process. It is revealed that cyanide stretch of [Ru-P4VP-CoFe]-post shifts to higher wavenumbers (2060 cm^{-1} to 2106 cm^{-1}), which is attributed to partial oxidation of Co^{2+} to Co^{3+} during photoexcitation (Figure 3.21). As pointed out by Galan-Mascaros et al., this change could also be due to linkage isomerism (CN bond flipping).[52] Furthermore, two major bands of pristine sample at 1417 cm^{-1} and 1597 cm^{-1}, which were attributed to C=C_{ring} and C=N_{ring} of pyridyl rings, also observed after catalysis (Figure 3.22). This indicates the absence of decomposition of [Ru-P4VP] structure.

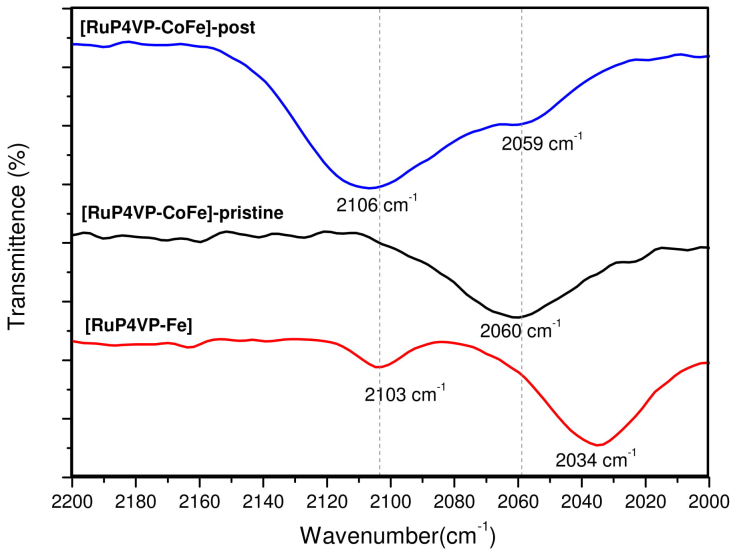

Figure 3.21: FTIR spectra of [Ru-P4VP-Fe], [Ru-P4VP-CoFe], and [Ru-P4VP-CoFe] after six catalytic cycle.

Although [Ru-P4VP-CoFe] assembly showed enhanced activity and stability compared to its intermolecular analogue system, comparison should also be made with dyad systems reported in literature. Photocatalytic activity is modest in comparison with Ru-based dyads reported by Thummel et al. (TON of 134 and 68)[13],[18] and trinuclear ruthenium assembly studied by Licheng Sun et al. (TON 38)[19]. However, as it was the goal of this thesis, dyads incorporating non-noble metals should be investigated in order to design cost-efficient PEC systems. In this respect, TON of 11 obtained with Ru-Co assembly presents a

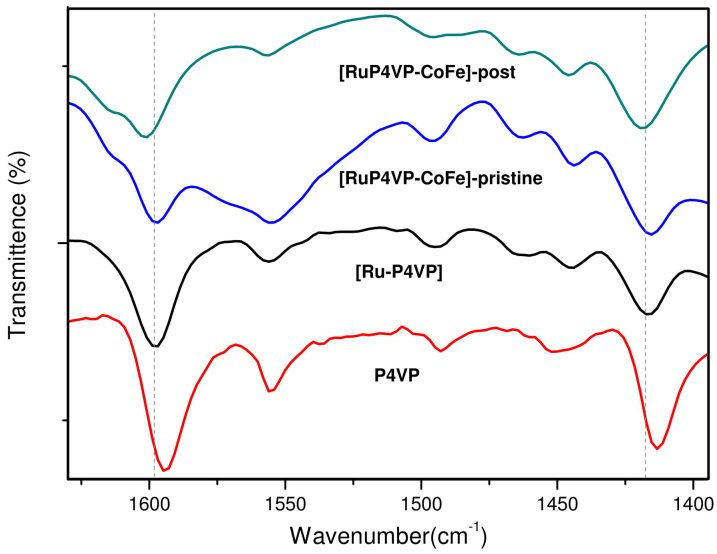

Figure 3.22: FTIR spectra of P4VP, [Ru-P4VP], [Ru-P4VP-CoFe], and [Ru-P4VP-CoFe] after six catalytic cycle.

valuable progress which also exhibits higher activity than Ru-Co dyad (TON of 5) reported by Licheng Sun et al.[21]. In terms of stability, the most extensive photocatalytic experiment reported in homogeneous environment is 70 min where [Ru-P4VP-CoFe] showed similar longevity without any decomposition. It is also important to underline that no studies have been reported so far on re-usability of dyads, and therefore this study is novel in the line of techniques to analyze catalytic performance of dyads.

Polymeric dyad assemblies presented in the literature are investigated in DSPEC systems where the assembly is anchored to a semiconductor. In such studies, the activities of the dyads are analyzed in different experimental conditions, and are reported in terms of current densities and faradaic efficiencies. For this reason, fair comparison of [Ru-P4VP-CoFe] system with polymeric dyads reported cannot be made.

3.2.2 [Co-P4VP] for Water Reduction

The cyclic voltammogram (CV) of [Co-P4VP] at a GCE in a H_2O/MeCN (1:1 v/v) mixture with 0.1 M of KNO_3 as a supporting electrolyte displays a redox potential at around -1.5 V (vs. $Fc^{+/0}$), which can be assigned to the $Co^{II/I}$ reduction process (Figure 3.23).

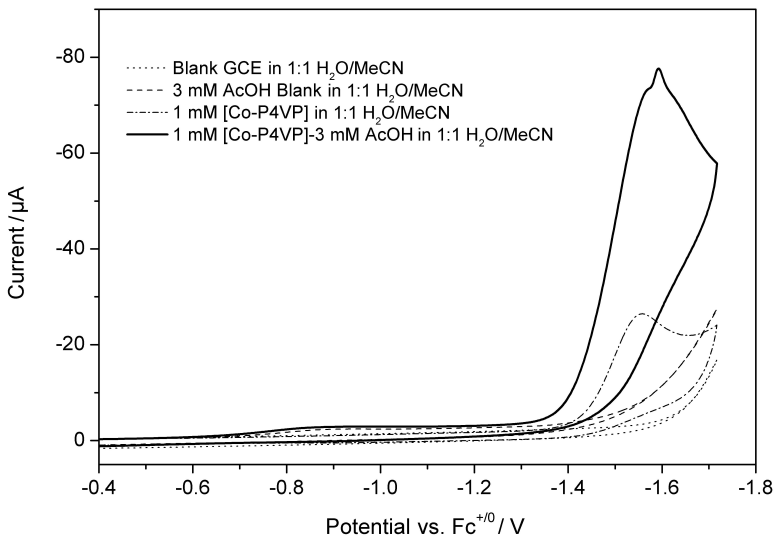

Figure 3.23: Comparison of CVs of blank (dot), 3 mM AcOH (dash), 1 mM [Co-P4VP] (1:5) (dash dot), and 1mM [Co-P4VP]- 3 mM AcOH (solid) in 1:1 H_2O/MeCN (v/v) mixture with 0.1 M KNO_3 at a GCE (ν: 100 mV s^{-1}).

The electrocatalytic proton reduction capacity of the [Co-P4VP] was studied in H_2O/MeCN mixture (1:1 v/v) after addition of AcOH as the proton source. CV of [Co-P4VP] with 3 mM of AcOH exhibits improved currents at more positive potentials closer to the $Co^{II/I}$ wave. Furthermore, CV experiments performed with GCE in the absence of catalyst, and acid did not exhibit any catalytic current. A modest increase in the current is observed when acid is added to the solution in the absence of a catalyst. Then, a significant current is observed with the addition of the acid in a solution of [Co-P4VP] (1 mM). The comparison of the CVs mentioned above suggests that [Co-P4VP] is responsible for the electrocatalytic H_2 evolution (Figure 3.23).

The CVs of the catalyst with and without acid are similar while a significantly higher current is obtained in the presence of [Co–P4VP]. CVs of $CoAc_2$ in H_2O/MeCN in the absence and the presence of 3 mM of AcOH were also obtained to compare the electrochemical behavior of the bare Co(II) precursor (Figure 3.24) and [Co-P4VP]. No significant increase in the current of $CoAc_2$ was observed compared to that of [Co-P4VP].

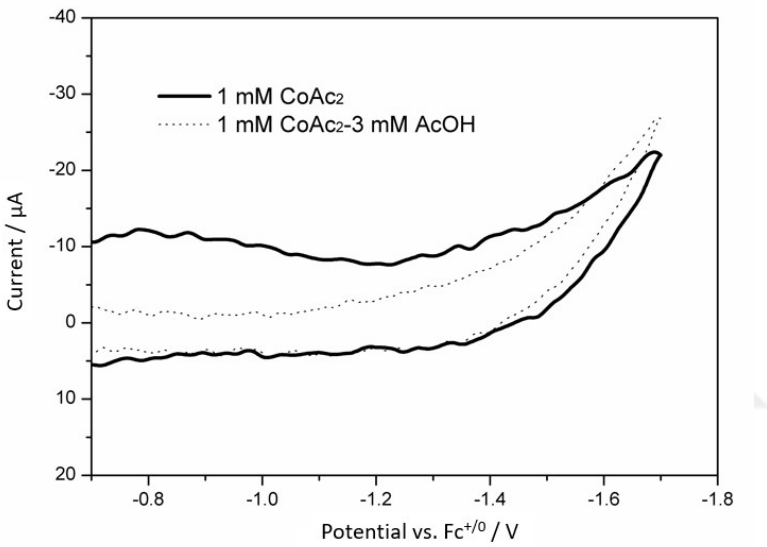

Figure 3.24: CVs of 1 mM of $[Co^{2+}]$ (solid) and 1 mM of $[Co^{2+}]$ in the presence of 3 mM of AcOH (dot) in 1:1 H_2O/MeCN (v/v) mixture containing 0.1 M of KNO_3 with a GCE.

Moreover, CV of a P4VP coated GCE was measured since P4VP is not soluble in 1:1 H_2O/MeCN (v/v) mixture. CVs of P4VP-coated GCE in a H_2O/MeCN mixture (1:1 v/v) containing 0.1 M KNO_3 supporting electrolyte with and without 3 mM of AcOH revealed that P4VP itself did not contribute significantly to the electrocatalytic activity (Figure 3.25). Overall, a comparison of CVs obtained for bare $CoAc_2$, bare P4VP, and [Co-P4VP] indicates that the target metallopolymer is the active catalyst in the presence of acid.

Electrochemical studies performed on [Co-P4VP] with different metal to ligand ratios of 1:5, 1:10, and 1:50 show similar electrochemical profiles (Figure 3.26). As it was discussed in earlier parts of the thesis, absorption spectra of these derivatives were similar as well (Figure 3.12). The aforementioned similarities

in these derivatives suggest that cobalt ions in [Co-P4VP] systems have similar coordination environments irrespective of the metal to ligand ratio.

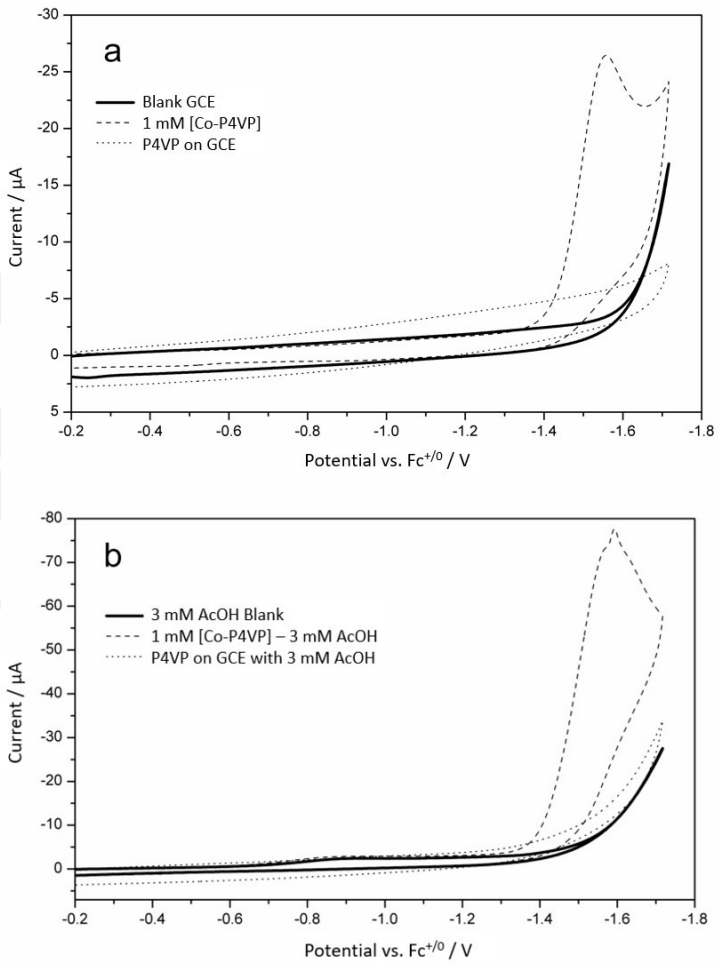

Figure 3.25: Comparison of CVs of P4VP coated GCE (dot) and blank GCE (solid). Also, these CV results were compared with solutions containing 1 mM [Co-P4VP] (dash) in 1:1 H_2O/MeCN (v/v) mixture with 0.1 M KNO_3 a) without AcOH b) with 3 mM AcOH (ν: 100 mV s^{-1}). For preparing P4VP on GCE, P4VP (5 mg) was resolved in dichloromethane solvent and 20 μL of this solution was dropped on GCE, then waited 5 minutes for drying at 80°C.

According to the literature, the overpotential for the catalytic water reduction process of the catalyst can be extracted from the lowest potential at which AcOH is reduced to dihydrogen.[69] The overpotential for [Co-P4VP] was derived as

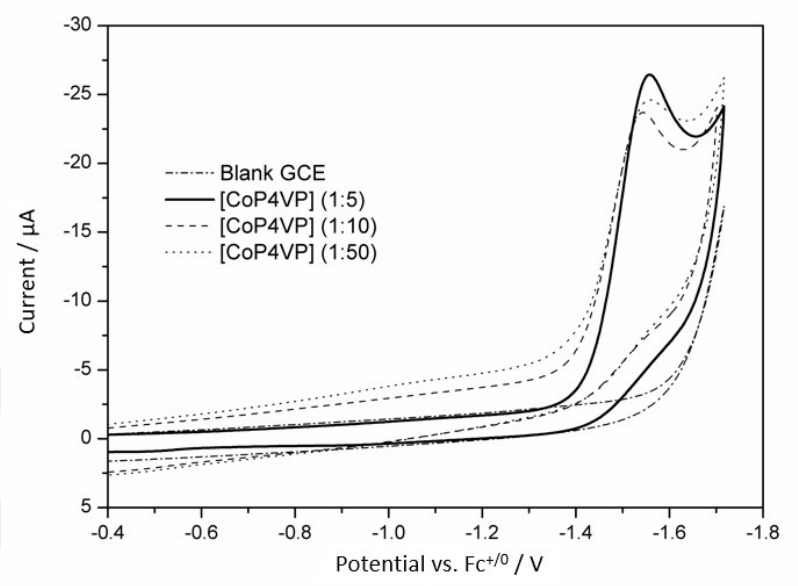

Figure 3.26: CVs comparison of [Co-P4VP] systems with different metal to ligand ratio, blank (dash-dot), 1:5 (solid), 1:10 (dash), and 1:50 (dot) in 1:1 H_2O/MeCN (v/v) mixture with 0.1 M KNO_3 with a GCE (ν: 100 mV s^{-1}).

approximately 210 mV when the half reaction potential for AcOH in MeCN is taken as 1.29 V vs. $Fc^{+/0}$.[70] The obtained overpotential is similar to the value reported for $[Co_3(C_6H_{11}O_2)_6][BF_4]_2$ (175 mV) [71] and much lower than the reported overpotential for $[Co(CF_3SO_3)$(1,4-di(picolyl)-7-(p-toluenesulfonyl)-1,4,7-triazacyclononane)$][CF_3SO_3]$ (590 mV)[69]. The comparison above is quite rough due to the assumption that pKa value of AcOH is identical in a H_2O/MeCN (1:1 v/v) mixture to that in MeCN since [Co-P4VP] is only partially soluble in pure H_2O and MeCN.

The peak current of the wave (I_p) obtained in the presence of [Co-P4VP] increases linearly with the square root of the scan rate ($\nu^{1/2}$), indicating a diffusion-controlled process (Figure 3.27).[72]

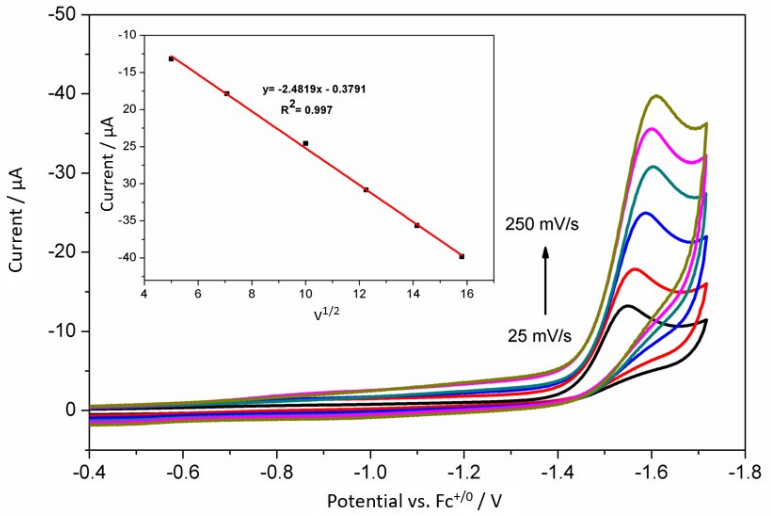

Figure 3.27: CVs of 1 mM of [Co-P4VP] (1:5) in 1:1 H_2O/MeCN (v/v) mixture with 0.1 M KNO_3 with a GCE at different scan rates (25-250 mV s^{-1}). The inset shows the linear dependence of the current on the square root of the scan rate.

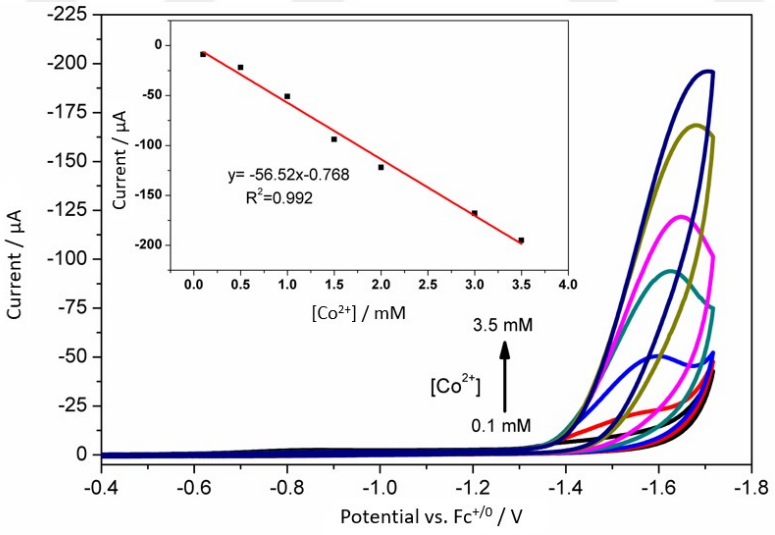

Figure 3.28: CVs of different concentrations of [Co-P4VP] (1:5) presence of 50 mM of AcOH in 1:1 H_2O/MeCN (v/v) mixture with 0.1 M KNO_3 with a GCE (ν: 100 mV s^{-1}). The inset shows the linear dependence of the current on the different concentrations of [Co-P4VP].

A series of CV measurements were performed to determine the rate order of the electrocatalysis with respect to [Co-P4VP] and AcOH. The electrocatalytic H_2

evolution capacity of [Co–P4VP] was investigated with increasing concentrations of AcOH. The linear trend in the current with increasing acid concentration is a clear indication of the electrocatalytic H_2 evolution (Figure 3.29). The deviation from linearity at acid concentrations of above 5 mM could be attributed to the deactivation of the complex. The electrode was polished before each CV scan to avoid the contribution from possible adsorbed species. CVs have two characteristic features; a broad band due to the molecular cobalt ion and an irreversible spike that indicates the presence of an adsorbed species. The maximum point just before the spike (labeled as *) was, thus, used to investigate the electrocatalytic activity of [Co–P4VP]. The electrochemical behavior of [Co–P4VP] since a deactivation process, which was discussed below in detail, is observed above an acid concentration of 3 mM and at relatively high negative overpotentials.

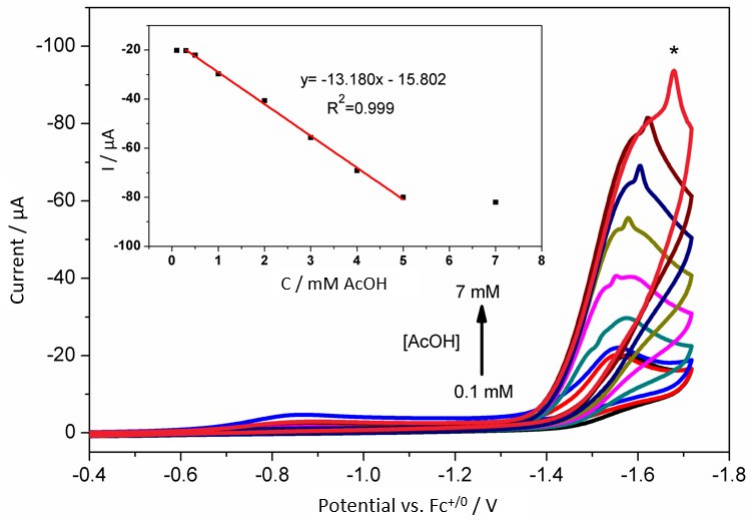

Figure 3.29: CVs of 1 mM of [Co-P4VP] (1:5) in 1:1 H_2O/MeCN (v/v) mixture with 0.1 M KNO_3 with a GCE in increasing concentrations of AcOH (0.1-7 mM) (ν: 50 m s^{-1}). The electrode is polished before each CV scan to avoid the contribution from a possible deposited species. The inset shows the linear dependence of the current on the increasing concentrations of AcOH.

The plot of the catalytic current (I_c) versus concentration of [Co–P4VP] also exhibits linearity. The electrochemical studies systematically performed with increasing concentrations of [Co-P4VP] and AcOH indicate that catalytic hydrogen generation is first-order with respect to the concentration of [Co-P4VP] and is second-order with respect to [AcOH] at low concentrations as extracted using

equation (3.1),

$$I_c = nFA[cat]\sqrt{Dk[H^+]^2} \tag{3.1}$$

where I_c is the catalytic current, n is the number of electrons, F is the Faraday constant, A is area of the electrode, [cat] is the concentration of catalyst, D is diffusion constant, k is rate constant, and $[H^+]$ is the concentration of the acid.[73] A second-order reaction rate with respect to the concentration of the acid and a first-order rate with respect to the concentration of the catalyst indicates the presence of a water reduction process that involves $2e^-$ and $2H^+$.

The turnover frequency (TOF) of the catalyst could be extracted by plotting the slopes of these lines against $\nu^{1/2}$ (Figure 3.30) for a catalytic process that involves an electron transfer followed by a catalytic reaction (E_rC_i' scheme).[73]

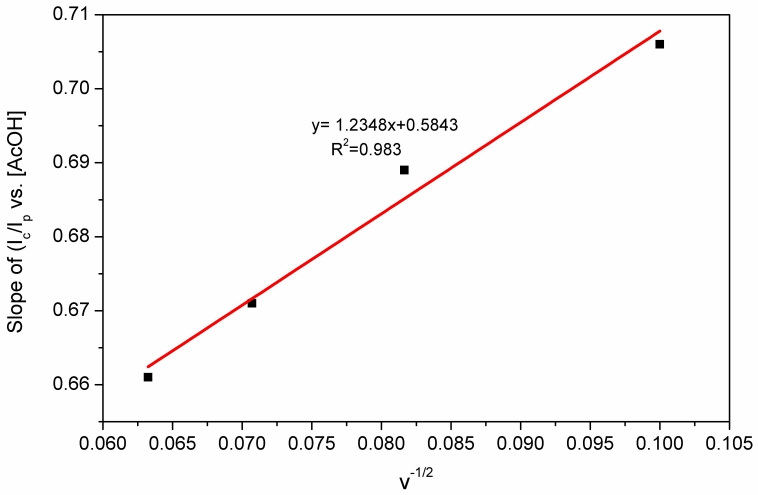

Figure 3.30: Plot of the slopes vs. $\nu^{-1/2}$. The linear fit is 1.2348x + 0.5843, R^2 = 0.983. For 60 mM [AcOH], this corresponds to TOF of ca. 35 mol H_2/ (mol [Co-P4VP] × h).

A linear trend is obtained from the I_c/I_p versus [AcOH] plots for different scan rates (where I_p is the peak current in the absence of acid) as presented in Figure 3.31.

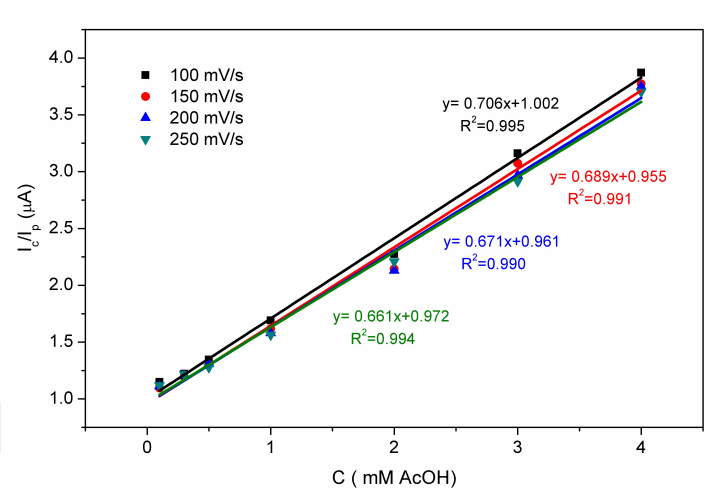

Figure 3.31: Plot of I_c/I_p as a function of [AcOH] for 1.0 mM of [Co-P4VP] in 1:1 H_2O/MeCN with 0.1 M KNO_3; with GCE at different scan rate (100-250 mV s^{-1}).

TOF for the catalyst in the presence of 60 mM of AcOH is calculated as 35 h^{-1}, by using Equation (3.2),

$$\frac{I_c}{I_p} = \frac{n}{0.4463}\sqrt{\frac{RTk[H^+]^2}{F\nu}} \tag{3.2}$$

where I_c is the catalytic current in presence of acid, I_p is the peak current in absence of acid, n is the number of electrons, R is the universal gas constant, T is temperature, k is rate constant, $[H^+]$ is the concentration of the acid, F is the Faraday constant, and ν is the scan rate. Result was similar to the value reported for the CoPy4 system.[73] Here, it should be noted that [Co-P4VP] is completely deactivated at acid concentrations above 5 mM. Although the system cannot operate at an acid concentration of 60 mM, the similar electrochemical behavior and catalytic performances of a cobalt polypyridyl system and [Co-P4VP] suggest the formation of a metallopolymer in [Co-P4VP] that incorporates single cobalt sites surrounded by pyridyl groups of P4VP. From the TOF value (35 mol H_2 / (mol [Co-P4VP] $\times$ h), H_2 evolution was calculated as 0.058 mmol mg^{-1} h^{-1},

which is higher than CoPy4 system (0.047 mmol mg^{-1} h^{-1})[74], cobalt(II) complex supported by 2-tetrahydrofurfurylamino-N,N-bis(2-methylene-4-tert-butyl-6-methyl)phenol (0.029 mmol mg^{-1} h^{-1})[75], MoS_2, and Ni2P (bulk) (0.038 and 0.039 mmol mg^{-1} h^{-1})[76], respectively. Furthermore, H_2 production rate for various catalysts is listed in Table 3.2.

Table 3.2: H_2 production rate for various catalysts

Catalyst	**Proton Source**	**TOF/mol H_2 mol^{-1} [catalyst]h^{-1}**	**H_2 production /mmol mg^{-1} h^{-1}**	**Over-potential/ mV**
CoPy4 [77]	Trifluoro-acetic acid	40	0.047****	400
LCoNCMe* [78]	Acetic acid	16.04	0.029****	889
MoS_2 [79]	Phosphotun-gstic acid	-	0.038	-
Ni2P [79]	Phosphotun-gstic acid	-	0.039	-
Co[(DPA-bpy) $(OH_2)](PF_6)_3$** [80]	Neutral phosphate buffer	410	0.67****	-
$CoA_2(H_2O)_2$*** [81]	Acetic acid	350.7	0.9	687.6
Co-P4VP	Acetic acid	35	0.058****	210

*Cobalt(II) complex supported by 2-tetrahydrofurfurylamino-N,N-bis(2-methylene-4-tert-butyl-6-methyl)phenol.
**Cobalt complex with N,N-bis(2-pyridinylmethyl)-2,2'-bipyridine-6-methanamine.
***Cobalt(II) complex with picolinic acid ions.
****Values were calculated using TOF and molecular weight of catalyst.

At low acid concentrations, the shape of the catalytic current wave is similar to the shape obtained in the absence of acid. However, I_c saturates at the concentrations above approximately 5 mM, and the rate of reaction becomes acid independent. Furthermore, an unusual irreversible spike labeled * was observed above acid concentrations of 3 mM that increases with increasing concentration of the acid. Such irreversible sharp peaks which have not

been observed in cobalt polypyridyl complexes previously reported in the literature are generally attributed to the adsorption of chemical species on the electrode surface (Figure 3.29).[74] Several studies have shown that cobalt complexes could act as precursors for the electrodeposition of nanoparticles to catalyze H_2 evolution.[47],[48],[49] Rinse tests are usually used in electro-supported catalysis to investigate whether catalytically active, insoluble, and strongly attached species are deposited onto the electrode surface.[75] Therefore, a rinse test was performed to investigate the composition of the deposits on the GCE. An electrolysis experiment at -1.5 V (vs. $Fc^{+/0}$) was performed with 1 mM of [Co-P4VP] H_2O/MeCN (1:1 v/v) solution in the presence of 5 mM of AcOH and 0.1 M of KNO_3 for 15 min using GCE (area: 0.071 cm^2) as the working electrode. The electrode was then rinsed with an H_2O/MeCN mixture to eliminate weakly attached molecular species and was placed into a 5 mM AcOH solution in the absence of the catalyst. A comparison of CV profiles for the blank GCE and the GCE that was used for electrolysis indicates that the deposit also serves as a catalyst for water reduction since the CV of rinsed electrode exhibits a higher cathodic current compared to that of the blank electrode (Figure 3.32). This result suggests that [Co-P4VP] transforms to cobalt-containing particles at more negative values than the potential of -1.1 V in acidic media.

Therefore, catalytic activity of Co particles coated onto an FTO electrode, [Co-coat@FTO] was also investigated. [Co-coat@FTO] were formed by electrolysis of a 1 mM of [Co-P4VP] in 1:1 H_2O/MeCN (v/v) mixture containing 3 mM of AcOH and 0.1 M of KNO_3 at -1.5 V (vs. $Fc^{+/0}$) for 2 h. The modified FTO electrode was then rinsed and used as the working electrode for further electrochemical measurements. Figure 3.33 shows the linear sweep voltammogram (LSV) of [Co-coat@FTO].

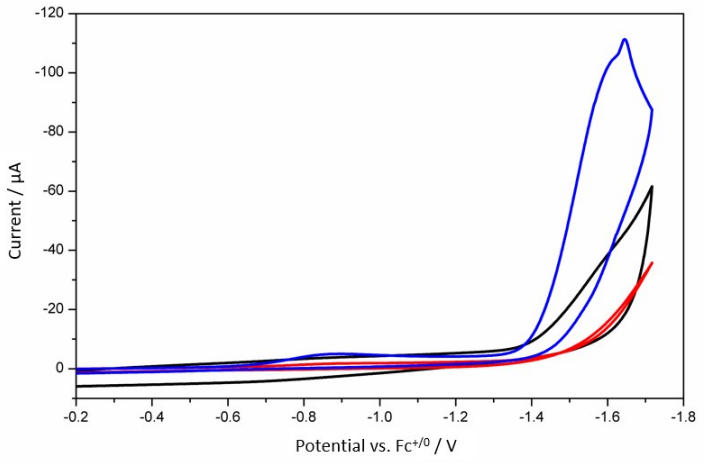

Figure 3.32: CV comparison of 3 mM AcOH (red line), 1mM [Co-P4VP] in the presence of 3 mM AcOH (blue line), and after rinse test (black line) at a GCE. For rinse test, electrolysis was performed for 15 min in 1 mM [Co-P4VP] with 5 mM AcOH in 1:1 H_2O /MeCN (v/v) mixture with 0.1 M KNO_3, and CV was recorded for the rinsed but unpolished electrode. Electrolyte solution: 5 mM AcOH in 1:1 H_2O /MeCN (v/v) mixture with 0.1 M KNO_3.

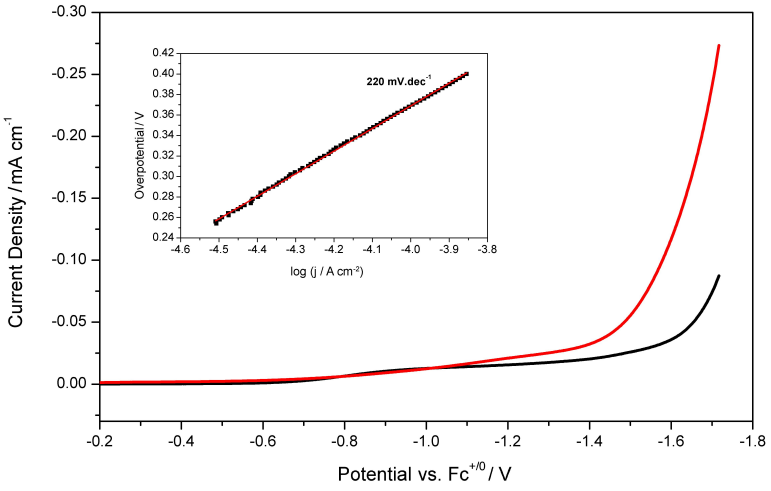

Figure 3.33: LSV of blank FTO (black line) and [Co-coat@FTO] (red line) obtained after electrolysis of 1 mM [Co-P4VP]-3 mM AcOH and H_2O/MeCN solution with 0.1 M KNO_3 at an applied potential of -1.5 V (vs. $Fc^{+/0}$) for 2 hours (ν: 100 mV s^{-1}). The inset shows Tafel slope derived from LSV.

A catalytic onset potential of 210 mV is required to produce a current density (j) of 55 μA cm^{-2}, and the Tafel slope of 220 mV dec^{-1} was derived from LSV analysis at a low scan rate. Although obtained at slightly different experimental conditions, the slope is similar to that of the Co nanoparticles electrodeposited from cobalt-bisglyoximato diphenyl complex solution (200 mV dec^{-1})[49], Co2B-500 (amorphous cobalt boride annealed at 500°C) (177 mV dec^{-1} at higher current density)[76], and Cu-TPA catalyst (copper(II) tris(2-pyridylmethyl)amine) (320 mV dec^{-1})[82], reported previously. A relatively high Tafel slope indicates that the mechanism of hydrogen evolution on [Co-coat@FTO] was similar to that of the Co nanoparticles and Co2B-500. Three classical theories are routinely used to explain the mechanisms underlying the evolution of hydrogen on metal surfaces. The first step of hydrogen evolution reaction (HER) is believed to be the proton discharge step (Volmer step, 120 mV dec^{-1}) followed by electrochemical desorption (Heyrovsky step, 40 mV dec^{-1}) or chemical desorption (Tafel step, 30 mV dec^{-1}).[83],[84] The water discharge reaction (Volmer step) appears to be the dominant rate limiting step during the HER with Co particles.[76] The exchange current density (j_0) of $10^{-2.67}$ mA cm^{-2} was determined from the Tafel plot and is similar to that obtained for Co nanoparticles electrodeposited from cobalt-bisglyoximato diphenyl complex ($10^{-2.7}$ mA cm^{-2}) [49], electrodeposited Co-based film ($10^{-2.5}$ mA cm$^{-2}_{geometric}$) [85], and higher than that for electropolymerized Co(II) dibenzotetraaza(14) annulene system ($10^{-4.70}$ mA cm$^{-2}_{geometric}$) [86].

A controlled potential electrolysis was also performed in a 1:1 H_2O/MeCN (v/v) solution with 0.1 M of KNO_3 containing 60 mM of AcOH at -1.5 V for the quantitative measurement of the evolved H_2. The results summarized in Figure 3.34 indicate that a total of around -17 C of charge passed during the course of 2 h while 1 C was collected during a 5 h experiment at -0.75 V versus NHE using Co nanoparticles prepared from boron-capped tris(glyoximato) cobalt clathrochelate [47], and 3 C of charge was obtained at -1 V versus SCE using a cobalt-bisglyoximato diphenyl complex [49]. It should be noted that the aforementioned studies were performed at different experimental conditions, making it difficult to make any comparisons.

A 100 μL aliquot of gas collected from the headspace of the electrolysis cell was

transferred with a gas-tight syringe to obtain a gas chromatogram (Figure 3.35). Current efficiency of 91% for H_2 production catalyzed by [Co-coat@FTO] was calculated using the moles of H_2 produced (0.081 mmol) and the charge passed (-17 C) during the electrolysis (Figure 3.34b). This clearly indicates that the Co-based particles formed during the electrolysis serve as the active species for H_2 evolution.

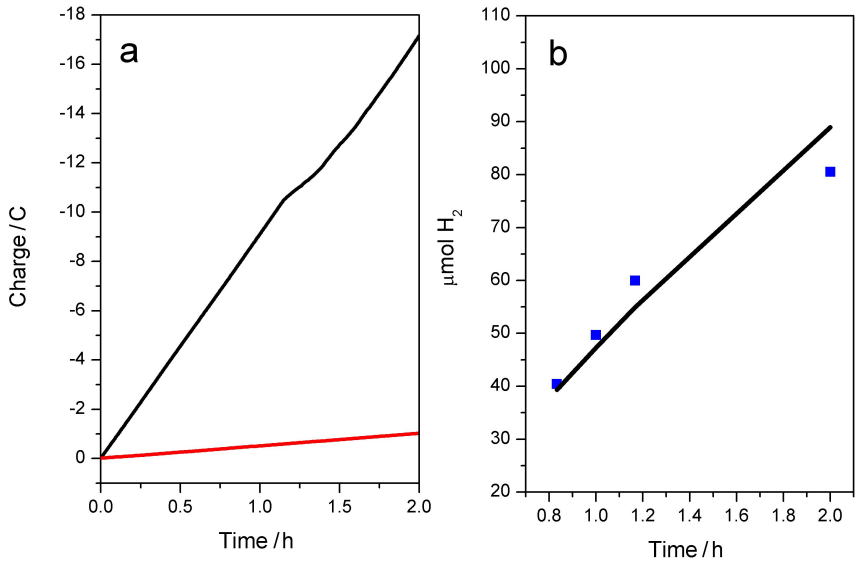

Figure 3.34: Controlled potential electrolysis at -1.5 V (vs. $Fc^{+/0}$) in 1:1 H_2O/MeCN with 0.1 M KNO_3 and 60 mM AcOH a) Charge vs. time blank FTO (red line) and [Co-coat@FTO] (black line). b) H_2 produced with [Co-coat@FTO] vs. time confirmed by GC. The quantity of H_2 (μmol) is integrated from GC (blue squares) and Faraday's Law assuming 91% Faraday's yield (black circles).

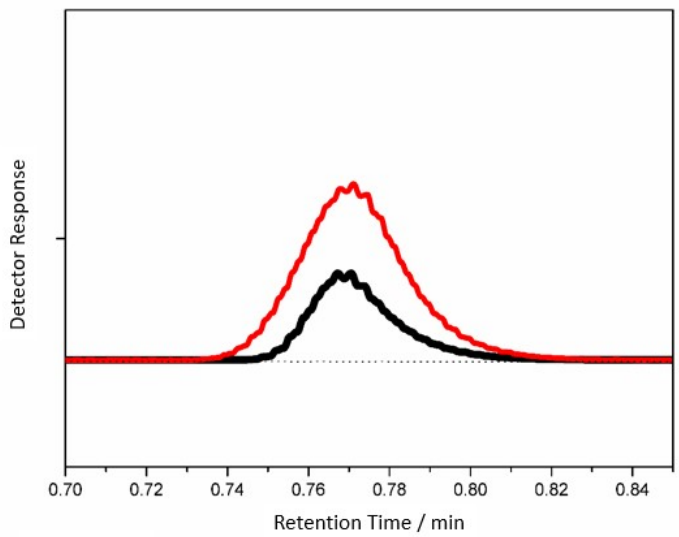

Figure 3.35: Gas chromatogram of a 100 μL aliquot of the headspace taken from a sealed electrochemical cell using a [Co-coat@FTO] working electrode at -1.5 V (vs. $Fc^{+/0}$) before (dotted line) and after (red line) 50 min of electrolysis. Also reference H_2 solution was shown black line.

Chapter 4

Conclusion

Towards the development of renewable and non-pollutant energy systems, utilization of water splitting is a key consideration for hydrogen production. In this respect, the goal of this thesis was to develop efficient, stable, and low-cost catalysts for two half reactions of water splitting; water oxidation and water reduction.

In the first part of this thesis, a photocatalyst for water oxidation was synthesized, characterized, and its catalytic performance was investigated. A novel heterogeneous PS-WOC dyad, incorporating poly(4-vinylpyridine) as a bridge between a ruthenium chromophore and a cobalt-based PBA, was presented. To our knowledge, it is the first study that the photocatalytic performance of a polymer bridged dyad is investigated in a homogeneous solution. The structure of the assembly was confirmed step by step, from Ru precursor to final product, with FTIR, UV-Vis, and XPS studies. EDX studies revealed the formation of a non-stoichiometric compound, wherein the atomic ratio of Ru to Fe atoms varies from 1.87 to 2.56. Nevertheless, a rough molecular formula of $Na_{0.97}Co_{2.86}[Fe(CN)_5]_{2.13}$-$[P4VP]_6$-$[Ru(bpy)_2]Cl_{2.89}$ was estimated by averaging the atomic ratios obtained at several different points. SEM and XRD studies indicated the formation small Prussian Blue cubic structures with around 50 nm size. Catalytic performance of the dyad was investigated under 1 h light illumination, and oxygen evolution was

measured with GC where pressure transducer was used as a supporting device to sense the pressure during the photocatalytic experiment. The dyad showed slightly higher catalytic activity (a TOF of 5.6 $\times$ 10^{-4} s^{-1}) compared to the relevant multi-component system (4.5 $\times$ 10^{-4} s^{-1}). Moreover, [Ru-P4VP-CoFe] exhibits higher activity than a previously reported molecular dyad system, which consists of a ruthenium-based chromophore and a cobalt-cubane catalyst.[21]

Important outcome of the study was the fact that dyad can be re-used up to six cycles without decomposition where the multi-component analogue can only be used for three cycles with a significant lose in the catalytic activity. It is noteworthy that no studies have been reported so far on re-usability of dyad systems, and therefore this study is a step forward in investigation techniques of such supramolecular assemblies. In a total of 6 h study, TON was obtained as 11 where 5-fold enhancement is achieved compared to its intermolecular analogue. Absence of any decomposition leading to an oxide species was confirmed by post-catalytic measurements with FTIR and XPS techniques. Catalytic and post-catalytic characterization studies revealed that the assembly is active for oxidizing water with relatively higher stability. Furthermore, a straightforward synthesis is presented compared to previously reported dyad systems since poly(4-vinylpyridine) is a commercially available ligand.

In the second part of the thesis, a cobalt based metallopolymer is proposed as an electrocatalyst for water reduction. Structure characterizations were conducted with UV-Vis, XPS and SEM techniques. At low acid concentrations, electrocatalytic activity for H_2 evolution process similar to cobalt polypyridyl complexes was observed. Overall, [Co-P4VP] assembly has following advantages over cobalt-polypyridyl complexes:

i) Facile synthesis method is achieved by using a commercially available polymer.

ii) Similar catalytic performance (TOF = 35 h^{-1}) is achieved in more demanding conditions (1:1 H_2O/MeCN (v/v) mixture and 60 mM AcOH)

where a cobalt polypyridyl system, Co^{II}-PY4 (2-bis(2-pyridyl)(methoxy)methyl-6-pyridylpyridine) in MeCN exhibits a TOF of 40 h^{-1} in the presence of 60 mM trifluoroacetic acid.[87]

iii) The diverse chemistry of polymers can be used further to tune the electrochemical stability of cobalt-polymer systems.

At high acid concentrations and cathodic potential above -1.1 V, [Co-P4VP] alters to cobalt based particles. Around 80 μmoles of H_2 gas was collected during the course of 2 hours of electrolysis at -1.5 V (vs. $Fc^{+/0}$) in 1:1 H_2O/MeCN and 60 mM AcOH, which is confirmed by both the amount of coulombs passed and gas chromatography. An exchange current density of $10^{-2.67}$ A cm^{-2} was obtained from Tafel slope, which is comparable with electrodeposited cobalt-based catalyst, electrodeposited Co-based film ($10^{-2.5}$ A cm^{-2})[87], and higher than that for electropolymerized Co(II) dibenzotetraaza(14) annulene system ($10^{-4.70}$ A cm^{-2}) [85],[86]. XPS studies indicate that [Co-coat@FTO] is composed of cobalt sites with multiple oxidation states that are surrounded with poly(4-vinylpyridine). Therefore, although exact coordination environment of cobalt ions in [Co-P4VP] system cannot be made, electrochemical profile of [Co-P4VP] shows that the use of metallopolymers is a viable and facile approach to prepare active electrocatalysts for H_2 evolution, and it can be a new direction for the development of efficient and robust catalysts for hydrogen evolution from water.

Bibliography

[1] G. Marbán and T. Valdés-Solís, "Towards the hydrogen economy?," *Int. J. of Hydrogen Energy*, vol. 32, no. 12, pp. 1625–1637, 2007.

[2] S. Dutta, "A review on production, storage of hydrogen and its utilization as an energy resource," *J. Ind. Eng. Chem.*, vol. 20, no. 4, pp. 1148–1156, 2013.

[3] P. Sharma and M. Kolhe, "Review of sustainable solar hydrogen production using photon fuel on artificial leaf," *Int. J. Hyrogen Energy*, vol. 42, no. 36, pp. 22704–22712, 2017.

[4] P. P. Edwards, V. Kuznetsov, W. David, and N. Brandon, "Hydrogen and fuel cells: Towards a sustainable energy future," *Energy Policy*, vol. 36, no. 12, pp. 4356–4362, 2008.

[5] O. Johansson, *Ruthenium(II) Polypyridyl Complexes: Applications in Artificial Photosynthesis*. PhD thesis, Stockholm University, 2004.

[6] E. S. Andreiadis, M. Chavarot-Kerlidou, M. FonteCave, and V. Artero, "Artificial photosynthesis: From molecular catalysts for light-driven water splitting to photoelectrochemical cells," *Photochem. Photobiol.*, vol. 87, no. 5, pp. 946–964, 2011.

[7] J. Barber, "Photosynthetic energy conversion: Natural and artificial," *Chem. Soc. Rev.*, vol. 38, no. 1, pp. 185–196, 2009.

[8] L. Duan, L. Tong, Y. Xu, and L. Sun, "Visible light-driven water oxidation—from molecular catalysts to photoelectrochemical cells," *Energy Environ. Sci.*, vol. 4, no. 9, p. 3296, 2011.

[9] D. G. Nocera, "The artificial leaf," *Acc. Chem. Res.*, vol. 45, no. 5, pp. 767–776, 2012.

[10] X. Sala, I. Romero, M. Rodriguez, L. Escriche, and A. Llobet, "Molecular catalysts that oxidize water to dioxygen," *Angew. Chemie - Int. Ed.*, vol. 48, no. 16, pp. 2842–2852, 2009.

[11] W. T. Eckenhoff, W. R. McNamara, P. Du, and R. Eisenberg, "Cobalt complexes as artificial hydrogenases for the reductive side of water splitting.," *Biochim. Biophys. Acta - Bioenerg.*, vol. 1827, no. 8-9, pp. 958–973, 2013.

[12] J. J. Concepcion, J. W. Jurss, P. G. Hoertz, and T. Meyer, "Catalytic and surface-electrocatalytic water oxidation by redox mediator-catalyst assemblies.," *Angew. Chemie - Int. Ed.*, vol. 48, no. 50, pp. 9473–9476, 2009.

[13] N. Kaveevivitchai, R. C. ad R. Zong, M. E. Ojaimi, and R. P. Thummel, "A molecular light-driven water oxidation catalyst.," *J. Am. Chem. Soc.*, vol. 134, no. 26, pp. 10721–10724, 2012.

[14] D. L. Ashford, M. K. Gish, A. K. Vannucci, M. K. Brennaman, J. L. Templeton, J. M. Papanikolas, and T. J. Meyer, "Molecular chromophore-catalyst assemblies for solar fuel applications.," *Chem. Rev.*, vol. 115, no. 23, pp. 13006–13049, 2015.

[15] M. Yamamato, L. Wang, F. Li, T. Fukushima, K. Tanaka, L. Sun, and H. Imahori, "Visible light-driven water oxidation using a covalently-linked molecular catalyst–sensitizer dyad assembled on a tio_2 electrode.," *Chem. Sci.*, vol. 7, no. 2, pp. 1430–1439, 2016.

[16] B. D. Sherman, D. L. Ashford, A. M. Lapides, M. V. Sheridan, K. R. Wee, and T. J. Meyer, "Light-driven water splitting with a molecular electroassembly-based core/shell photoanode.," *J. Phys. Chem. Lett.*, vol. 6, no. 16, pp. 3213–3217, 2015.

[17] B. D. Sherman, Y. Xie, M. V. Sheridan, D. Wang, T. J. Meyer, and J. J. Concepcion, "Light-driven water splitting by a covalently linked ruthenium-based chromophore-catalyst assembly.," *ACS Energy Lett.*, vol. 2, no. 1, pp. 124–128, 2017.

[18] L. Kohler, N. Kaveevivitchai, R. Zong, and R. P. Thummel, "Component analysis of dyads designed for light-driven water oxidation.," *Inorg. Chem.*, vol. 53, no. 2, pp. 912–921, 2014.

[19] F. Li, Y. Jiang, B. Zhang, F. Huang, Y. Gao, and L. S. and, "Towards a solar fuel device: Light-driven water oxidation catalyzed by a supramolecular assembly.," *Angew. Chemie - Int. Ed.*, vol. 51, no. 10, pp. 2417–2420, 2012.

[20] G. Leem, B. D. Sherman, and K. S. Schanze, "Polymer - based chromophore – catalyst assemblies for solar energy conversion.," *Nano Converg.*, vol. 4, no. 1, p. 37, 2017.

[21] X. Zhou, F. Li, H. Li, B. Zhang, F. Yu, and L. Sun, "Photocatalytic water oxidation by molecular assemblies based on cobalt catalysts.," *ChemSusChem.*, vol. 7, no. 9, pp. 2453–2456, 2014.

[22] J. Jiang, B. D. Sherman, Y. Zhao, R. He, I. Ghiviraga, L. Alibabaei, T. J. M. amd G. Leem, and K. S. Schanze, "Polymer chromophore-catalyst assembly for solar fuel generation.," *ACS Appl. Mater. Interfaces.*, vol. 9, no. 23, pp. 19529–19534, 2017.

[23] D. M. Ryan, M. K. Coggins, J. J. Concepcion, D. L. Ashford, Z. Fang, L. Alibabaei, D. Ma, T. Meyer, and M. L. Waters, "Synthesis and electrocatalytic water oxidation by electrode-bound helical peptide chromophore-catalyst assemblies.," *Inorg. Chem.*, vol. 53, no. 15, pp. 8120–8128, 2014.

[24] S. E. Bettis, D. M. Ryan, M. K. Gşsh, L. Alibabaei, T. J. Meyer, M. L. Waters, and J. M. Papanikolas, "Photophysical characterization of a helical peptide chromophore-water oxidation catalyst assembly on a semiconductor surface using ultrafast spectroscopy.," *J. Phys. Chem. C*, vol. 118, no. 12, pp. 6029–6037, 2014.

[25] Z. Fang, A. Ito, H. Luo, D. L. Ashford, J. J. Concepcion, L. Alibabaei, and T. J. Meyer, "Polypyridyl ru(ii)-derivatized polypropylacrylate polymer with a terminal water oxidation catalyst. application of reversible addition–fragmentation chain transfer polymerization.," *Dalt. Trans.*, vol. 44, no. 18, pp. 8640–8648, 2015.

[26] H. Shimakoshi, M. Nishi, A. Tanaka, K. Chikama, and Y. Hisaeda, "Photocatalytic function of a polymer-supported b12 complex with a ruthenium trisbipyridine photosensitizer.," *Chem. Commun. (Camb).*, vol. 47, no. 23, pp. 6548–6555, 2011.

[27] G. Leem, Z. A. Morseth, K. R. Wee, J. Jiang, M. K. Brennaman, J. M. Papanikolas, and K. S. Schanze, "Polymer-based ruthenium(ii) polypyridyl chromophores on tio$_2$ for solar energy conversion.," *Chem. Asian J.*, vol. 11, no. 8, pp. 1257–1267, 2016.

[28] M. L. Helm, M. P. Stewart, R. M. Bullock, M. R. DuBois, and D. L. DuBois, "A synthetic nickel electrocatalyst with a turnover frequency above 100,000 s^1 for h$_2$ production.," *Science (80-.).*, vol. 333, no. 6044, pp. 863–866, 2011.

[29] D. Z. Zee, T. Chantarojsiri, J. R. Long, and C. J. Chang, "Metal-polypyridyl catalysts for electro- and photochemical reduction of water to hydrogen.," *Acc. Chem. Res.*, vol. 48, no. 7, pp. 2027–2036, 2015.

[30] W. T. Eckenhoff, W. R. McNamara, P. Du, and R. Eisenberg, "Cobalt complexes as artificial hydrogenases for the reductive side of water splitting.," *Biochim. Biophys. Acta - Bioenerg.*, vol. 1827, no. 8-9, pp. 958–973, 2013.

[31] J. R. McKone, S. C. Marinescu, B. S. Brunschwig, J. R. Winkler, and H. B. Gray, "Earth-abundant hydrogen evolution electrocatalysts.," *Chem. Sci.*, vol. 5, no. 3, pp. 865–878, 2014.

[32] S. Losse, J. G. Vos, and S. Rau, "Catalytic hydrogen production at cobalt centres.," *Coord. Chem. Rev.*, vol. 254, no. 21-22, pp. 2492–2504, 2010.

[33] P. Du and R. Eisenberg, "Catalysts made of earth-abundant elements (co, ni, fe) for water splitting: Recent progress and future challenges.," *Energy Environ. Sci.*, vol. 5, no. 3, p. 6012, 2012.

[34] N. Queyriaux, R. T. Jane, J. Massin, V. Artero, and M. Chavarot-Kerlidou, "Recent developments in hydrogen evolving molecular cobalt(ii)-polypyridyl catalysts.," *Coord. Chem. Rev.*, vol. 304-305, pp. 3–19, 2015.

[35] J. L. Dempsey, B. S. Brunschwig, J. R. Winkler, and H. B. Gray, "Hydrogen evolution catalyzed by cobaloximes.," *Acc. Chem. Res.*, vol. 42, no. 12, pp. 1995–2004, 2009.

[36] M. Razavet, V. Artero, and M. Fontecave, "Proton electroreduction catalyzed by cobaloximes: Functional models for hydrogenases.," *Inorg. Chem.*, vol. 44, no. 13, p. 4786–4795, 2005.

[37] B. Reuillard, J. Warnan, J. J. Leung, D. W. Wakerley, and E. Reisner, "A poly(cobaloxime)/carbon nanotube electrode: Freestanding buckypaper with polymer-enhanced h_2-evolution performance.," *Angew. Chemie - Int. Ed.*, vol. 55, no. 12, p. 3952–3957, 2016.

[38] N. Kaeffer, M. Chavarot-Kerlidou, and V. Artero, "Hydrogen evolution catalyzed by cobalt diimine-dioxime complexes.," *Acc. Chem. Res.*, vol. 48, no. 5, p. 1286–1295, 2015.

[39] R. S. Khnayzer, V. S. Thoi, M. Nippe, A. E. King, J. W. Jurss, K. A. E. Roz, J. R. Long, C. J. Chang, and F. N. Castellano, "Towards a comprehensive understanding of visible-light photogeneration of hydrogen from water using cobalt(ii) polypyridyl catalysts.," *Energy Environ. Sci.*, vol. 7, no. 4, p. 1477, 2014.

[40] A. Rodenberg, M. Orazietti, B. Probst, C. Bachmann, R. Alberto, K. K. Baldridge, and P. Hamm, "Mechanism of photocatalytic hydrogen generation by a polypyridyl-based cobalt catalyst in aqueous solution.," *Inorg. Chem.*, vol. 54, no. 2, pp. 646–657, 2015.

[41] M. Vennampalli, G. Liang, L. Katta, C. E. Webster, and X. Zhao, "Electronic effects on a mononuclear co complex with a pentadentate ligand for catalytic h_2 evolution.," *Inorg. Chem.*, vol. 53, no. 19, p. 10094–10100, 2014.

[42] J. Y. Yang, R. M. Bullock, M. R. DuBois, and D. L. DuBois, "Fast and efficient molecular electrocatalysts for h_2 production: Using hydrogenase enzymes as guides.," *MRS Bull.*, vol. 36, no. 1, pp. 39–47, 2011.

[43] D. H. Pool and D. L. DuBois, "$[ni(pph_2nar_2)_2(ncme)][bf_4]_2$ as an electrocatalyst for h_2 production: Pph_2nar_2=1,5-(di(4-(thiophene-3-yl)phenyl)-3,7-diphenyl-1,5-diaza-3,7-diphosphacyclooctane).," *J. Organomet. Chem.*, vol. 694, no. 17, p. 2858–2865, 2009.

[44] J. Seo, R. T. Pekarek, and M. J. Rose, "Photoelectrochemical operation of a surface-bound, nickel-phosphine h_2 evolution catalyst on p-si(111): A molecular semiconductor—catalyst construct.," *Chem. Commun.*, vol. 51, no. 68, pp. 4–7, 2015.

[45] Y. Sun, C. Liu, D. C. Grauer, J. Yano, J. R. Long, P. Yang, and C. J. Chang, "Electrodeposited cobalt-sulfide catalyst for electrochemical and photoelectrochemical hydrogen generation from water.," *J. Am. Chem. Soc.*, vol. 135, no. 47, p. 17699–17702, 2013.

[46] N. Kaeffer, A. Morozan, J. Fize, E. Martinez, L. Guetaz, and V. Artero, "The dark side of molecular catalysis: Diimine-dioxime cobalt complexes are not the actual hydrogen evolution electrocatalyst in acidic aqueous solutions.," *ACS Catal.*, vol. 6, no. 6, p. 3727–3737, 2016.

[47] E. Anxolabéhère-Mallart, C. Cıstentin, M. Fournier, S. Nowak, M. Robert, and J. M. Savéant, "Boron-capped tris(glyoximato) cobalt clathrochelate as a precursor for the electrodeposition of nanoparticles catalyzing h_2 evolution in water.," *J. Am. Chem. Soc.*, vol. 134, no. 14, p. 6104–6107, 2012.

[48] S. E. Ghachtouli, M. Fournier, S. Cherdo, R. Guillot, M. F. Charlot, E. Anxolabéhère-Mallart, M. Robert, and A. Aukauloo, "Monometallic cobalt-trisglyoximato complexes as precatalysts for catalytic h2 evolution in water.," *J. Phys. Chem.*, vol. 117, no. 33, p. 17073–17077, 2013.

[49] E. Anxolabéhère-Mallart, C. Costentin, M. Fournier, and M. Robert, "Cobalt-bisglyoximato diphenyl complex as a precatalyst for electrocatalytic h 2 evolution.," *J. Phys. Chem.*, vol. 118, no. 25, p. 13377–13381, 2014.

[50] S. E. Ghachtouli, R. Guillot, F. Brisset, and A. Aukauloo, "Cobalt-based particles formed upon electrocatalytic hydrogen production by a cobalt pyridine oxime complex.," *ChemSusChem*, vol. 6, no. 12, p. 2226–2230, 2013.

[51] D. Martin, B. D. McCarthy, C. L. Donley, and J. L. Dempsey, "Electrochemical hydrogenation of a homogeneous nickel complex to form a surface adsorbed hydrogen-evolving species.," *Chem. Commun. (Camb).*, vol. 51, pp. 2–5, 2014.

[52] S. Goberna-Ferrón, W. Y. Hernández, B. Rodríguez-García, and J. R. Galán-Mascarós, "Light-driven water oxidation with metal hexacyanometallate heterogeneous catalysts.," *ACS Catal.*, vol. 4, no. 6, p. 1637–1641, 2014.

[53] E. P. Alsaç, E. Ülker, S. V. K. Nune, Y. Dede, and F. Karadas, "Tuning the electronic properties of prussian blue analogues for efficient water oxidation electrocatalysis: Experimental and computational studies.," *Chem. Eur. J.*, vol. 24, no. 19, p. 4856–4863, 2018.

[54] M. Aksoy, S. V. K. Nune, and F. Karadas, "A novel synthetic route for the preparation of an amorphous co/fe prussian blue coordination compound with high electrocatalytic water oxidation activity.," *Inorg. Chem.*, vol. 55, no. 9, p. 4301–4307, 2016.

[55] Z. Kap, E. Ülker, S. V. K. Nune, and F. Karadas, "Electrocatalytic hydrogen evolution with cobalt–poly(4-vinylpyridine) metallopolymers.," *J. Appl. Electrochem.*, vol. 48, no. 2, p. 201–209, 2018.

[56] A. Devadoss, A. M. Spehar-Délèze, D. A. Tanner, P. Bertoncello, R. Marthi, T. E. Keyes, and R. J. Forster, "Enhanced electrochemiluminescence and charge transport through films of metallopolymer-gold nanoparticle composites.," *Langmuir*, vol. 26, no. 3, p. 2130–2135, 2010.

[57] C. F. Hogan and R. J. Forster, "Mediated electron transfer for electroanalysis: Transport and kinetics in tin films of [ru $(bpy)_2pvp_{10}$] $(clo_4)_2$.," *Analytica Chimica Acta*, vol. 396, pp. 13–21, 1999.

[58] D. J. Kenney, T. P. Flynn, and J. B. Gallini, "Reactions of ferropentacyanamines.," *Inorg. Nucl. Chem.*, vol. 20, no. 1-2, pp. 75–81, 1961.

[59] N. Kazuo, *Infrared and Raman Spectra of Inorganic and Coordination Compounds*. John Wiley & Sons, 1986.

[60] K. R. Dunbar and R. A. Heintz, *Chemistry of Transition Metal Cyanide Compounds: Modern Perspectives*. John Wiley & Sons, 1997.

[61] S. A. Jannuzzi, B. Martins, M. I. Felisberti, and A. L. B. Formiga, "Supramolecular interactions between inorganic and organic blocks of pentacyanoferrate/poly(4-vinylpyridine) hybrid metallopolymer.," *J. Phys. Chem.*, vol. 116, no. 51, p. 14933–14942, 2012.

[62] V. Marin, E. Holder, and U. S. Schubert, "Polymeric ruthenium bipyridine complexes: New potential materials for polymer solar cells.," *J. Polym. Sci. Part A Polym. Chem.*, vol. 42, no. 2, p. 374–385, 2004.

[63] B. Durham, J. V. Caspar, J. K. Nagle, and T. J. Meyer, "Photochemistry of tris(2,2'-bipyridine)ruthenium(2+) ion.," *J. Am. Chem. Soc.*, vol. 104, no. 18, p. 4803–4810, 1982.

[64] V. Leigh, W. Ghattas, R. Lalrempuia, H. Müller-Bunz, M. T. Pryce, and M. Albrecht, "Synthesis, photo, and electrochemistry of ruthenium bis(bipyridine) complexes comprising a n- heterocyclic carbene ligand.," *Inorg. Chem.*, vol. 52, no. 9, p. 5395–5402, 2013.

[65] N. S. McIntyre and M. G. Cook, "X-ray photoelectron studies on some oxides and hydroxides of cobalt, nickel, and copper.," *Anal. Chem.*, vol. 47, no. 13, p. 2208–2213, 1975.

[66] F. Hegner, I. Herraiz-Cardona, D. Cardenas-Morcoso, N. Lopez, J. R. Galan-Mascaros, and S. Gimenez, "Cobalt hexacyanoferrate on $bivo_4$ photoanodes for robust water splitting.," *ACS Appl. Mater. Interfaces*, vol. 9, no. 43, pp. 37671–37681, 2017.

[67] Y. Mulyana, K. G. Alley, K. M. Davies, B. F. Abrahams, B. Moubaraki, K. S. Murray, and C. Boskovic, "Dinuclear cobalt(ii) and cobalt(iii) complexes of bis-bidentate napthoquinone ligands.," *Dalt. Trans.*, vol. 43, no. 6, p. 2499–2511, 2014.

[68] T. Katoh, G. Imamura, S. Obata, and K. Saiki, "Growth of n-doped graphene from nitrogen containing aromatic compounds: The effect of precursors on the doped site.," *RSC Adv.*, vol. 6, no. 16, p. 13392–13398, 2016.

[69] A. Call, Z. Codolà, F. Acuña-Parés, and J. Lloret-Fillol, "Photo- and electrocatalytic h_2 production by new first-row transition-metal complexes based on an aminopyridine pentadentate ligand.," *Chem. Eur. J.*, vol. 20, no. 20, p. 6171–6183, 2014.

[70] V. Fourmond, P.-A. Jacques, M. Fontecave, and V. Artero, "H_2 evolution and molecular electrocatalysts: Determination of overpotentials and effect of homoconjugation.," *Inorg. Chem*, vol. 49, no. 22, pp. 10338–10347, 2010.

[71] H. S. Ahn, T. C. Davenport, and T. D. Tilley, "Molecular cobalt electrocatalyst for proton reduction at low overpotential.," *Chem. Commun.*, vol. 50, no. 29, p. 3834–3837, 2014.

[72] A. D. Wilson, R. H. Newell, M. M. J., J. T. Muckerman, M. R. DuBois, and D. L. DuBois, "Hydrogen oxidation and production using nickel-based molecular catalysts with positioned proton relays.," *J. Am. Chem. Soc.*, vol. 128, no. 1, p. 358–366, 2006.

[73] J. P. Bigi, T. E. Hanna, W. H. Harman, A. Chang, and C. J. Chang, "Electrocatalytic reduction of protons to hydrogen by a water-compatible cobalt polypyridyl platform.," *Chem. Commun.*, vol. 46, no. 6, p. 958–960, 2010.

[74] J. W. Jurss, J. C. Concepcion, M. R. Norris, J. L. Templeton, and T. J. Meyer, "Surface catalysis of water oxidation by the blue ruthenium dimer.," *Inorg. Chem.*, vol. 49, no. 9, p. 3980–3982, 2010.

[75] C. C. L. McCrory, C. Uyeda, and J. C. Peters, "Electrocatalytic hydrogen evolution in acidic water with molecular cobalt tetraazamacrocycles.," *J. Am. Chem. Soc.*, vol. 134, no. 6, p. 3164–3170, 2012.

[76] J. Masa, P. Weide, D. Peeters, I. Sinev, W. Xia, Z. Sun, C. Somsen, M. Muhler, and W. Schuhmann, "Amorphous cobalt boride (co_2b) as a highly efficient nonprecious catalyst for electrochemical water splitting: Oxygen and hydrogen evolution.," *Adv. Energy Mater.*, vol. 6, no. 12, p. 1502313, 2016.

[77] J. P. Bigi, T. E. Hanna, W. H. Harman, A. Chang, and C. J. Chang, "Electrocatalytic reduction of protons to hydrogen by a water-compatible cobalt polypyridyl platform.," *Chem. Commun.*, vol. 46, no. 6, p. 958–960, 2010.

[78] C.-N. Lin, L.-L. Zhou, L.-Z. Fu, S.-Z. Zhan, and C.-H. Chen, "Synthesis, structure and electrochemical properties of a cobalt(ii) complex supported by 2-tetrahydrofurfurylamino-n,n-bis(2-methylene-4-tert-butyl-6-methyl)phenol.," *Inorganic Chemistry Communications*, vol. 61, pp. 97–99, 2015.

[79] L. MacDonald, J. C. McGlynn, N. Irvine, I. Alshibane, L. G. Bloor, B. Rausch, J. S. J. Hargreaves, and L. Cronin, "Using earth abundant materials for the catalytic evolution of hydrogen from electron-coupled-proton-buffers.," *Sustainable Energy Fuels*, vol. 1, pp. 1782–1787, 2017.

[80] W. M. Singh, T. Baine, S. Kudo, S. Tian, X. A. N. Ma, H. Zhou, N. J. DeYonker, T. C. Pham, J. C. Bollinger, D. L. Baker, B. Yan, C. E. Webster, and X. Zhao, "Electrocatalytic and photocatalytic hydrogen production in aqueous solution by a molecular cobalt complex.," *Angew. Chem. Int. Ed.*, vol. 51, p. 5941 –5944, 2012.

[81] L.-Z. Fu, L.-Z. Tang, Y.-X. Zhang, Q.-N. Liang, C. Fang, and S.-Z. Zhan, "Hydrogen evolution catalyzed by a water-soluble cobalt(ii) complex with picolinic acid ions.," *International Journal of Hydrogen Energy*, vol. 41, pp. 249–254, 2016.

[82] X. Liu, H. Zheng, Z. Sun, A. Han, and P. Du, "Earth-abundant copper-based bifunctional electrocatalyst for both catalytic hydrogen production and water oxidation.," *ACS Catal.*, vol. 5, no. 3, p. 1530–1538, 2015.

[83] K. Zeng and D. Zhang, "Recent progress in alkaline water electrolysis for hydrogen production and applications.," *Prog. Energy Combust. Sci.*, vol. 36, no. 3, pp. 307–326, 2010.

[84] M. S. Faber and S. Jin, "Earth-abundant inorganic electrocatalysts and their nanostructures for energy conversion applications.," *Energy Environ. Sci.*, vol. 7, p. 3519–3542, 2014.

[85] S. Cobo, J. Heidkamp, P.-A. Jacques, J. Fize, V. Fourmond, L. Guetaz, B. Jousselme, V. Ivanova, H. Dau, S. Palacin, M. Fontecave, and V. Artero, "Earth-abundant inorganic electrocatalysts and their nanostructures for energy conversion applications.," *Nat. Mater.*, vol. 11, no. 9, p. 802–807, 2012.

[86] S. Rioual, B. Lescop, F. Quentel, and F. Gloaguen, "A molecular material based on electropolymerized cobalt macrocycles for electrocatalytic hydrogen evolution.," *Phys. Chem. Chem. Phys.*, vol. 17, no. 20, p. 13374–13379, 2015.

[87] J. P. Bigi, T. E. Hanna, W. H. Harman, A. Chang, and C. J. Chang, "Electrocatalytic reduction of protons to hydrogen by a water-compatible cobalt polypyridyl platform.," *Chem. Commun.*, vol. 46, no. 6, p. 958–960, 2010.